Electrostatic field calculations related to electron lenses

John Coffey, Cheshire, UK.

2023

Key words: Coulomb's law, electric field, potential, Laplace's equation, charge density on conducting rectangle, disc, strip, annulus, cylinder lens, finite elements, analytic functions

1 Introduction

Many years ago I needed to make an electrostatic electron gun to fire low energy electrons at a perfectly clean metal target in an ultra-high vacuum, and examine the energy spectrum of the back-scattered scattered electrons at various angles. At that time the design of the gun was made using data in textbooks on electron optics including that by Klemperer[1], with some empirical adjustments. The gun was a simple device with a heated tungsten cathode emitting electrons, an anode to attract them and give them momentum, and a simple lens made of three coaxial cylindrical tubes each with a different voltage applied. In such designs the electric field from one tube protrudes into the internal space of its neighbour and will radially deflect electrons which are travelling more or less parallel to the axis so they cross the axis within a small region approximating a focal point. A single pair of adjacent tubes therefore forms a primitive lens component, and three tubes form a useful combination capable of focusing an electron beam onto a target a fixed distance away over a range of electron energies.

Though the electric potential satisfies Laplace's equation (in the absence of 'space charge' due to a heavy density of other electrons), analytic solutions of this partial differential equation can be found only for a small number of cases. These case are important because they are exact and so can be used to assess and calibrate approximate solutions. In a general case of practical interest, however, an approximate technique for quantifying the field distribution is necessary. Over the many years since my gun was made, finite element techniques have developed to allow more accurate values for the electric potential and field distributions. I have therefore decided to revisit this well studied and probably obsolete subject for no reason other than to satisfy my curiosity.

Calculations for lens design require these steps:

[1] 'Electron Optics' by Otto Klemperer, 2nd edn 1953. The 3rd edition published 1971 by Cambridge Univ Press with co-author M E Barnett.

1. specification and then iteration of the geometrical arrangement of the conducting surfaces and the voltages applied to each,
2. solution of Laplace's equation subject to the boundary conditions,
3. specification of the emitting surface: its geometry and the energy distribution of emitted electrons,
4. calculation of the trajectories of a sample of electrons,
5. parametrising the lens by its principle planes and aberrations, as in light optics,
6. allowance if necessary for space charge.
7. comparison of theory with the measured performance on the completed, possibly prototype, gun, and tweaking to tune performance.

This article is the first in what may perhaps become a short series giving my account of these matters. It deals only with electric potential distributions and fields which are either simple or have some relevance to electrostatic electron lenses. Whether I will write a further article on particle trajectories and hence the focusing properties of lenses remains to be seen. A fairly recent book[2] on the optics of electron lenses is by Douglas Heddle who I once met at York University. It gives detailed coverage of the design of these instruments. There is a well-developed commercial software package called SIMION for calculating electric fields and the trajectories of charged particles at *www.simion.com*.

§2 reminds the reader of some essential physics such as Coulomb's law and the fields of simple arrangements of charge. §3 examines potential distributions in rectangular coordinates such as a rectangular duct, developing both analytic solutions and solving the same problems with finite elements. §4 does much the same of systems which have cylindrical symmetry such as the electron lens made from two axially aligned cylindrical tubes. The section also deals with a uniform ring of charge and uses it to derive the fields around a non-conducting disc and a conducting disc. Appendix 1 supplies additional mathematical detail. §5 is about the distribution of electric charge over conducting bodies, particularly the disc, the infinite strip and the annulus. In this section and in Appendices 2 and 3 I explain a numerical model I have developed for obtaining the charge distribution. I have found only one other paper[3] dealing with the annulus, so my approach may be new. I had developed and written up my method before coming across this early paper.

2 Essential physics

2.1 Coulomb and Gauss's Laws

Classical physics pictures 'point charges' as infinitesimally small particles bearing a charge Q which is either 'positive' or 'negative', whatever these mean at a deeper level. A proton is

[2] 'Electrostatic Lens Systems', 2nd Edition by D W O Heddle, CRC Press, 2000.

[3] 'Calculation of the capacitance of a circular annulus by the method of subareas', T J Higgins and D K Reitan, AIEE Trans. Vol 70, 1951, p926

essentially a classical positive point charge with value $+e = 1{\cdot}602 \times 10^{-19}$ coulombs in SI units. A single electron is a point negative charge of $-e$. The interaction between charges Q_1 and Q_2 in free space is given by Coulomb's law

$$\mathbf{F} = \frac{Q_1 Q_2}{4\pi\varepsilon_0 r^2}\mathbf{u_r} \tag{1}$$

where $\mathbf{F}$ is the force, $\mathbf{u_r}$ the unit vector along the line joining the two charges, and r the distance between them. The law encompasses the fact that unlike charges attract one another, like ones repel; in Eq 1 a positive force is repulsive. The constant ε_0 is the permittivity of free space with the value $8{\cdot}854{\times}10^{-12}$ farads per metre. The combined constant is $1/(4\pi\varepsilon_0) = \kappa_C \approx 9{\times}10^9$ mF^{-1}. In much of this article I will assume units in which $\kappa_C = 1$ to save having to include it in every formula.

An electron will move according to Newton's laws subject to the net Coulomb forces from other charges. The usual way of looking at the aggregate force is to regard other charges as contributing to the electric field $\mathbf{E}(x, y, x)$ at each position (x, y, z):

$$\mathbf{E} = \kappa_C \sum_j^N \frac{Q_j}{r_j^2}\ \mathbf{u_{r_j}}.$$

The concept of a test charge Q is that it is so small that it causes no perturbation of the field, and simply accelerates under the net force $\mathbf{F}(x, y, z) = Q\mathbf{E}(x, y, z)$. The electric field is conservative, meaning that no net work is done when the test charge moves in any closed path within the field and returns to its starting point. Because of this $\mathbf{E}$ can be described by a scalar potential function V, measured in volts. The electric field is the negative gradient of the potential, and the repulsive force on a positive test charge Q is $Q\mathbf{E}$:

$$\mathbf{E} = -\nabla V, \qquad \mathbf{F} = -Q\,\nabla V. \tag{2a}$$

The corollary to this is that potential is given by the line integral of the projection of $\mathbf{E}$ along any path $\mathbf{p}$ from the position at which V is taken to be zero:

$$V = \int_0^P \mathbf{E} \cdot d\mathbf{p}. \tag{2b}$$

The dot $\cdot$ refers to the scalar product. $V(P)$ is the work done in moving a unit reference charge from the position of zero potential to position P. Clearly constant potential means zero electric field and zero net applied force. Since only the electric field has physical reality, the absolute value of potential has no particular significance, so any convenient position can be taken as having zero potential. Where possible this is usually a point infinitely far away.

Gauss' law states that, for any closed volume Ω, the integral of the flux of electric field flowing out of a closed volume is proportional to the total charge enclosed.

$$\iint_\Omega \mathbf{E}\, d\Omega = 4\pi\kappa_C Q \equiv \frac{Q}{\varepsilon_0}.$$

In differential form this is one of the Maxwell equations: that the divergence of the electric field at every point is equal to the value of the charge Q enclosed within a notional elementary cell around that point:

$$div\,\mathbf{E} \equiv \nabla \cdot \mathbf{E} = \frac{Q}{\varepsilon_0} \;=\; -div\ grad\ V \equiv -\nabla^2 V.$$

2.2 Conductors

The conductivity of real materials varies from almost ideal insulators (diamond) to almost ideal conductors (silver), depending on the ability of charges within and on the surface of the material to migrate. I will not deal with dielectrics because they are not relevant to electrons moving in a vacuum. In a conductor the more energetic electrons are free to move with thermal motion and to drift over the material lattice of ion cores in response to applied charges. Since the electrons in this mobile 'sea' repel each other, they will move to even out any perturbations and move as far from each other as possible. For this reason charge resides entirely on the outside of a conductor. Since there is then no net force on any electrons inside the metal, the electric field strength throughout the metal is zero and the voltage throughout is constant. Just outside the conductor the electric field is everywhere normal to its surface. When the conductor is attached to a battery or electrostatic generator, charges move onto the surface and spread out, and the potential of its surface increases. The density of electric charge over the surface of a conductor is in general not uniform but depends on its shape. More highly curved convex areas have higher charge density to maintain the potential constant. This is because at a highly curved position the component of electric force parallel to the surface, repelling electrons, is smaller, so more can gather together. Similarly, concave parts have lower charge density. At a sharp edge pointing into an external field the local density is effectively infinite, which is why lightning will strike a lightning conductor rather than a smoothly domed roof. The higher charge density causes a higher electric field at these positions according to Gauss's law. The redistribution of charge minimises the potential energy of the system (Thomson's theorem). The calculation of charge density distributions is discussed in §5.

The behaviour of a conductor depends on whether it is

- electrically insulated, or connected to earth or to a battery,
- placed in an external field or in a field-free space.

Points to note include

1. If it was charged before being isolated and is in a field-free space, it will create around it its own field. The ratio of the charge to surface potential, Q_A/V, is a constant property of the geometry called the 'capacitance' of the conductor. For instance, the capacitance of an isolated sphere of radius a is a, and of a disc is $2a/\pi$. Capacitance is a measure of the ability of the arrangement to store charge, and increases greatly when several conductors are placed close to each other.
2. A conductor in an external field will perturb that field because the potential over its surface will immediately attain a constant value. Charges flow inside the metal and

redistribute themselves to cancel the applied field on and throughout the metal. The redistribution can be pictured as new charges being 'induced' on the surfaces to oppose the applied field. Induced charges will appear whatever charge was initially given to the conductor.

3. If a conductor is connected to earth (ground), its potential can be taken as zero whatever field is applied. This is because the earth is effectively an infinite source and sink of charge, so mobile charges (mainly electrons) can flow into or out from the conductor to maintain it at the same potential. Much the same applies when the conductor is connected to a battery or other power supply, the other terminal of which is connected to earth.

4. A conductor which is electrically isolated is said to be 'floating' because its potential is not specified by being connected to earth or an external battery, but rather 'floats' to some value determined by the charge it carries and its position and orientation in the external field. Its potential can in principle be calculated by iteration in which the charge upon it is calculated from Gauss's law by integrating the electric field strength around its boundary. I do not consider such cases further.

2.3 Simple fields: Laplace's equation

Simple electric fields are listed below. Some formulae are derived in Appendix 1.

- single point charge q: $\mathbf{E} = q/r^2\,\mathbf{u}_r$, potential $-q/r$. Both field and potential $\to 0$ as $r \to \infty$. It is natural to take the zero of potential to be at infinite distance.

- a dipole, whether the two charges are of the same sign or opposite. The pattern of equipotentials is similar in the 2-D case of two parallel lines of charge, and contour plots are shown for this case in Figure 1. Note how when the charges are equal (right panel), the equipotential at 0 crosses itself in a figure-of-8.

- a conducting infinite plane with surface charge density σ (on each face). Consider a unit cube outside one surface of the conductor with one of its square faces coincident with unit area of the conductor. The enclosed charge is σ so, by Gauss's law and the symmetry of the situation, flux of $\mathbf{E}$ is σ/ε_0, the field being only in the z direction, normal to the surface. This is independent of distance from the plate provided it is effectively infinite. The potential varies linearly as $\sigma z/\varepsilon_0 + V_{reference}$.

- two large parallel plane metal surfaces held at different potentials. If the plates are d apart and one is at V_0 volts, the other at $V_1 > V_0$, $\mathbf{E} = (V_1 - V_0)/d$: potential $-(V_1 - V_0)x/d$ where x is the distance from one plate.

- line of charge. This being a 1-dimensional problem, the field $\mathbf{E}$ must vary as $1/r$ where r is the distance from the line. Let the charge density be λ per unit length and consider the contribution to the field at (r, z_0) from an element δz at $(0, z)$. Appendix 1 details how the components parallel and perpendicular to the line are taken and the integrals carried out. The field strength is $E = \kappa_C\,\lambda/r$, directly normal to the line, and the potential is $V = \kappa_C\,\lambda \ln r$. Though the field falls to zero as $r \to \infty$, the potential tends to infinity as

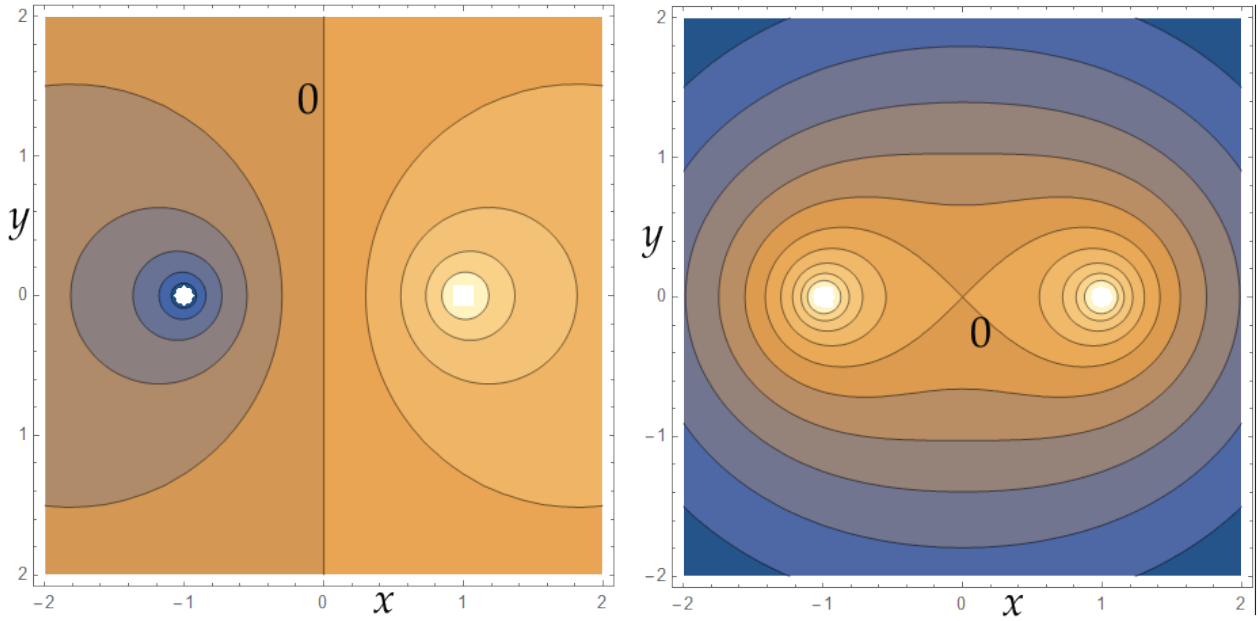

Figure 1: Equipotentials of two parallel lines of charge 2 units apart. Left: opposite polarity, right: same polarity.

$-\ln r$. This is because the line of charge itself is infinite. For this reason a point in space must be chosen where the potential has a reference value, and potentials at all other points referred to this; only potential differences are physically significant.

- circular ring of change. This is derived in §4.2 and elaborated in Appendix 1.

In the case of the two parallel plates, a proton released from rest on the surface of the V_1 plate would accelerate towards the other, taking a straight line trajectory. The situation is analogous to a stone falling with constant acceleration from a height to ground under the influence of gravity. Similarly, a charge injected at some angle to the parallel plates will follow a parabolic trajectory until it hits the attracting plate, just as a stone thrown into the air will follow a parabolic trajectory before coming to earth.

The potential distribution amongst an assembly of charged conducting surfaces satisfies Laplace's equation

$$\nabla^2 V = 0, \qquad \nabla^2 = \frac{\partial^2}{\partial x^2} + \frac{\partial^2}{\partial y^2} + \frac{\partial^2}{\partial z^2}. \tag{3}$$

Analytic solutions of this classic equation have been found for several simple cases. Indeed, much of 19th century applied mathematics was directed to solving this equation in important geometries. Curvilinear co-ordinate systems are employed – rectangular, cylindrical, spherical, and spheroidal. In cases of high symmetry solutions can be found in the form of a product of three independent functions, each depending on only one space co-ordinate. A three-dimensional problem is thereby split into three independent ordinary differential equations, one in each of the curvilinear co-ordinates. The solutions for V therefore generally take the form of a sum over products of 'special functions' peculiar to the co-ordinate system for that geometry. Thus products of sine and cosine trigonometric and hyperbolic functions occur

in rectangular co-ordinates, Bessel functions in situations with cylindrical symmetry, and Legendre and other spherical harmonics in spherical co-ordinates. Some of these analytic solutions are examined in the following sections. In all solutions the contours of constant potential are at right angles to the local electric field. The roles of equipotentials and field lines can be reversed so that the solution of the same equation also describes a system in which conductors have the shape of the field lines.

A further significant point is that Laplace's equation is linear so the principle of superposition applies: if $F_1(x, y, z)$ is a solution satisfying boundary conditions D_1 and $F_2(x, y, z)$ is a distinct solution satisfying boundary conditions D_2, then $F_1 + F_2$ is also a solution satisfying conditions $D_1 + D_2$. This follows directly from the potential of several point charges being additive.

3 Solutions of Laplace's equation in rectangular co-ordinates

3.1 A rectangular box

This is illustrated in Figure 2. It shows the cross-section of a uniform rectangular tube along the z axis whose four sides are electrically insulated from one another by thin gaps at the corners, and which are raised to voltages V_0 to $V3$. This is a two-dimensional problem:

$$\frac{\partial^2 V}{\partial x^2} + \frac{\partial^2 V}{\partial y^2} = 0$$

subject to the specified voltages on the four sides. Any linear function of x and y will have zero second derivatives. Observe also that $V = \exp \alpha x$ satisfies $d^2V/dx^2 = \alpha^2 V$ for any α, positive or negative, real on imaginary. Hence $V = \exp(\alpha x)\exp(\beta y)$ satisfies $\nabla^2 V = 0$ in the two dimensions x and y, provided $\beta^2 = -\alpha^2$. We may therefore work on the hypothesis that the solution to our box problem is a sum involving linear functions and functions of the form $A\exp(\pm\alpha(x \pm iy))$ where each α is a complex number determined by the geometry:

$$V = (c_1 + c_2 x)(c_3 + c_4 y) + \sum_k A_k \exp(\alpha_k(x + iy). \qquad (4a)$$

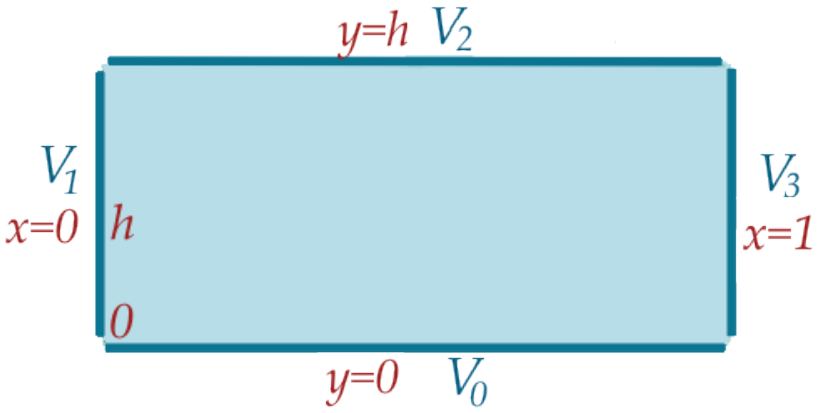

Figure 2: Cross section of a rectangular duct, width 2, height $2h$, whose sides may be at different potentials.

It is more convenient to cast the complex exponential into trigonometric and hyperbolic functions so we will work with

$$V = (c_1 + c_2x)(c_3 + c_4y) + \sum_k [A_k \cos(\alpha_k x)\cosh(\alpha_k y) + B_k \cos(\alpha_k x)\sinh(\alpha_k y) + C_k \sin(\alpha_k x)\cosh(\alpha_k y) + D_k \sin(\alpha_k x)\sinh(\alpha_k y)]. \quad (4b)$$

Since $V = 0$ at $y = 0$, the $\cosh(\alpha y)$ terms must be zero, and so must c_3. The general solution simplifies to

$$V = (c_1 + c_2x)c_4y + \sum_k [B_k \cos(\alpha_k x) + D_k \sin(\alpha_k x)]\sinh(\alpha_k y). \quad (4c)$$

Case 1 : Set $V_0 = V_1 = V_3 = 0$, $V_2 = 100$ volts: that is, the bottom and two vertical sides are all at 0 volts and the top plate is at 100 V. The potential is symmetric about $x = 0 \cdot 5$ so only terms in $\sin \alpha_j x$ are required. $\sin \alpha_k x = 0$ when $x = 1$ so $\alpha_k = k\pi$. Also $c_1 = c_2 = 0$. This leaves only the coefficients D_k to be found so that $V = V_2 = 100$ V at $y = h$. The solution has taken the form of a Fourier series along the line $y = h$ with coefficients $D_k \sinh(k\pi h$. Using the orthogonality of the sine functions

$$\int_{x_0}^{x_0+2\pi} \sin(jx)\sin(kx)\,dx = \begin{cases} \pi & \text{if } j = k \\ 0 & \text{if } j \neq k \end{cases}, \qquad \int_0^1 \sin^2(j\pi x)dx = \tfrac{1}{2},$$

$$\int_0^1 V_2 \sin(j\pi x)dx = \sum_k D_k \sinh(k\pi h) \int_0^1 \sin(k\pi x)\sin(j\pi x)dx = \tfrac{1}{2} D_j \sinh(j\pi h).$$

The left integral is zero if j is even and $2V_2/(j\pi)$ if odd. So let $j = 2n + 1$ and the potential within the rectangle is

$$V = \frac{4V_2}{\pi} \sum_{n=0}^{\infty} \frac{\sin((2n+1)\pi x)}{2n+1} \frac{\sinh((2n+1)\pi y)}{\sinh((2n+1)\pi h)}. \quad (5)$$

A contour plot at 10V intervals and 3-D graph of the voltage is shown in Figure 3.

The potential distribution can also be calculated by finite element methods. I have used the program Mecway 18 (*www.mecway.com*) to calculate contours for the case just examined, and the agreement with Figure 3 is indistinguishable to the eye. The series in Eq 5 was summed to 40 terms, and the FEA used a 16 by 16 grid of hex 20 elements. The four conducting surfaces were separated at the corners by a small insulated gap. Some numerical comparisons are listed in Table 1, which shows that at the mesh nodes selected the agreement is excellent. However, to use the FEA results for calculating electron trajectories, the field value and its derivatives are required at arbitrary points, and this requires interpolation between the mesh points. The first step would be to locate the finite element in which the point of interest is contained, and that would require a search of tabulated values covering all mesh elements.

Case 2 : Set $V_0 = 0$, $V_1 = V_3 = 30$, $V_2 = 100$ volts. We expect the 30 V contour to be a horizontal line between the left and right plates, dividing the square into two sections which are essentially mirror images of each other though scaled to ranges of 70 V and 30 V respectively. The contours in each sections are simply scaled version of those in Figure 3. The finite element calculation in Figure 4 confirms this intuitive assessment.

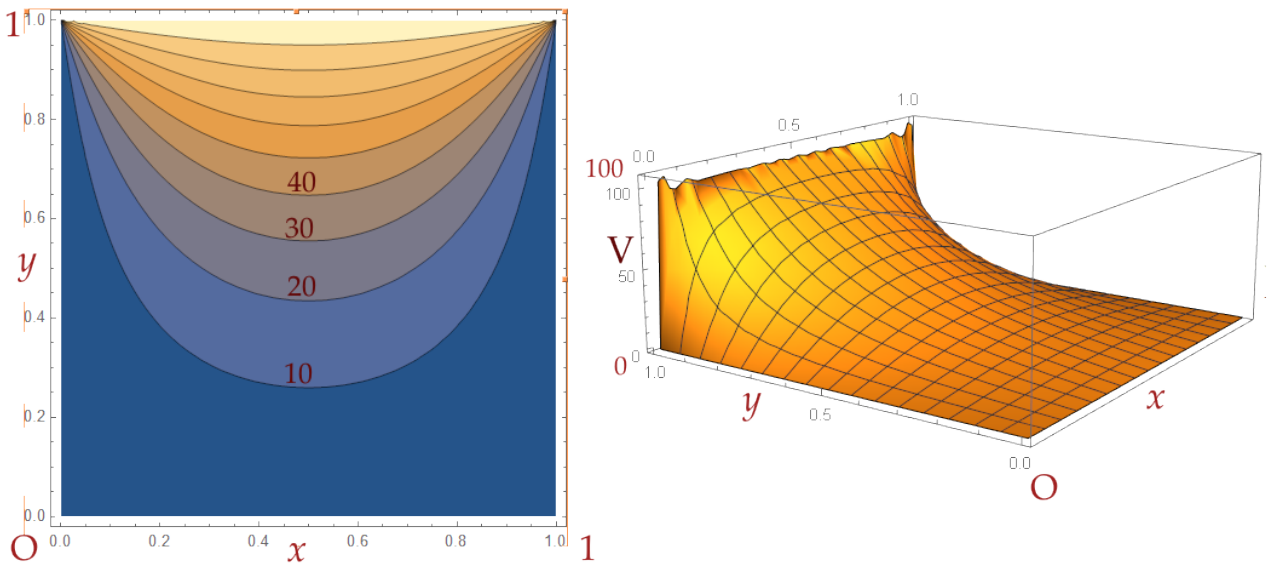

Figure 3: Voltage contours in rectangle (square) of Figure 2 for h = 1, V_0 = V_1 = V_3 = 0, V_2 = 100 V. Series summed to n = 40.

x	y	V (theory)	V (FEA)
0.50	0.50	25.0	24.99998
0.25	0.50	18.2028	18.20354
0.50	0.875	75.4269	75.42495
0.75	0.75	43.2028	43.20254

Table 1: Comparison of analytical theory and finite element analysis (FEA) of Figure 2.

Case 3 : Set V_0 = V_1 = 0, V_2 = V_3 = 100 volts. This case is symmetrical about the diagonal between points (0,1) and (1,0) which divides the square into two right-angled triangles. There are at least two approaches to solving for this potential distribution. In one, use is made of the principle that the field inside many polygons can be found by first mapping the interior of the polygon conformally into the upper half plane, solving the simpler problem there, then transforming the solution back to the polygon. The conformal transformation for this is the well known one by Schwarz and Christoffel. However, except for the simplest polygons with one or two angles, the method requires the integration of generally very complicated functions. An account with particular attention to the triangle and the rectangle has been given by Hendrik[4]. In the other approach, use is made of the principle of superposition. We already have the field when three sides are at 0 volts, the top at 100 V. If this is turned clockwise through 90 degrees, we have the right side at 100 V, the others at 0 V. Adding the two solutions gives the required field. Figure 5 shows in its left panel the potential contours by this superposition. It uses Eq 5 as stated and Eq 5 with x and y interchanged. I have also examined this case by finite elements. The results is given in the right panel of Figure 5. Again the comparison is remarkably good.

[4]'The Scharz-Christoffel transformation and elliptic functions' by W. H. Hendrik. Thesis, University of Groningen, 2009.

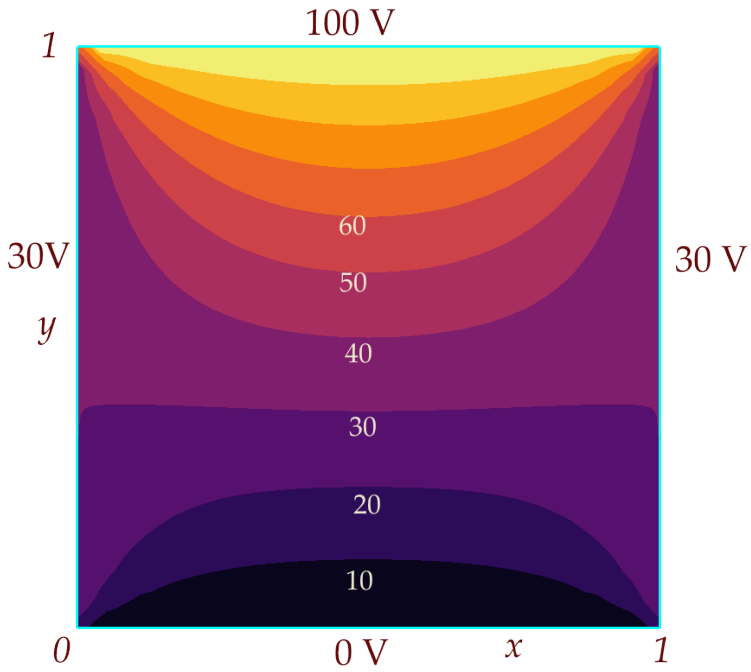

Figure 4: Finite element calculation of the potential distribution when side plates are at 30 V.

Case 4 : Set $V_0 = 0$, $V_1 = 20$, $V_2 = 100$, $V_3 = 65$ volts. This is an example of the general case in which are four conducting sides of the square have different applied potentials. An analytical solution is found by superposition of three rotated and voltage-scaled copies of Figure 3. The finite element method also readily yields a solution – Figure 6.

3.2 Infinite and semi-infinite plates

The two cases in this subsection can be solved using the Schwarz-Christoffel conformal transformation mentioned above. The transformation formula is calculated as follows. Suppose there is a polygon in real 2-D physical space plotted on the complex plane for which the variable is w – that is, the co-ordinates of the vertices are given as values of w. Let the internal angles of this polygon be β_1, β_2, ... These can take any values between 0 to 2π radians. The interior of this general polygon can be mapped into the complex upper half-plane for which the variable is z by the map

$$\frac{dw}{dz} = A(z - z_1)^{\beta_1/\pi - 1}(z - z_2)^{\beta_2/\pi - 1}(z - z_3)^{\beta_3/\pi - 1}.... \tag{6}$$

z_k are points along the real z axis to which the vertices are mapped. Though this theorem is quite striking in its generality, the difficulty in practice is in integrating Eq 6 to find w in terms of z. Most cases cannot be done.

Case 1 : A semi-infinite conducting plate parallel to an infinite plate separated by a gap of width h and at a different potential. The geometry is shown in Figure 7. The internal angles of the contrived and distorted but still valid 'polygon' are 0 and 2π radians. Let these map

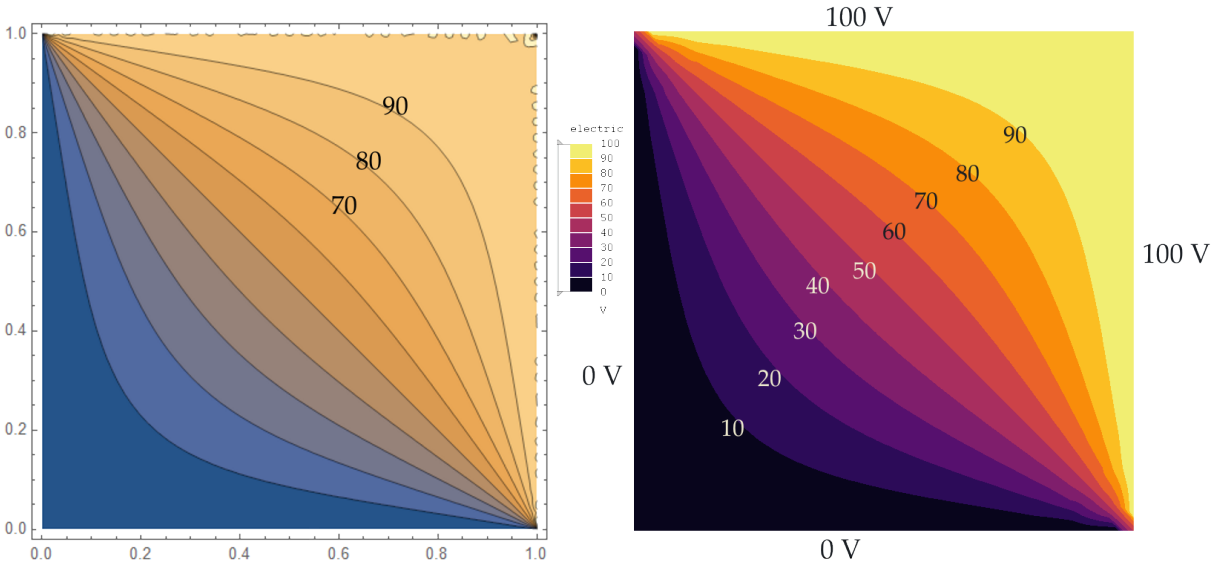

Figure 5: Equipotentials for a square with two adjacent sides at 0 V, two at 100 V. Left: theory, Right: FEA.

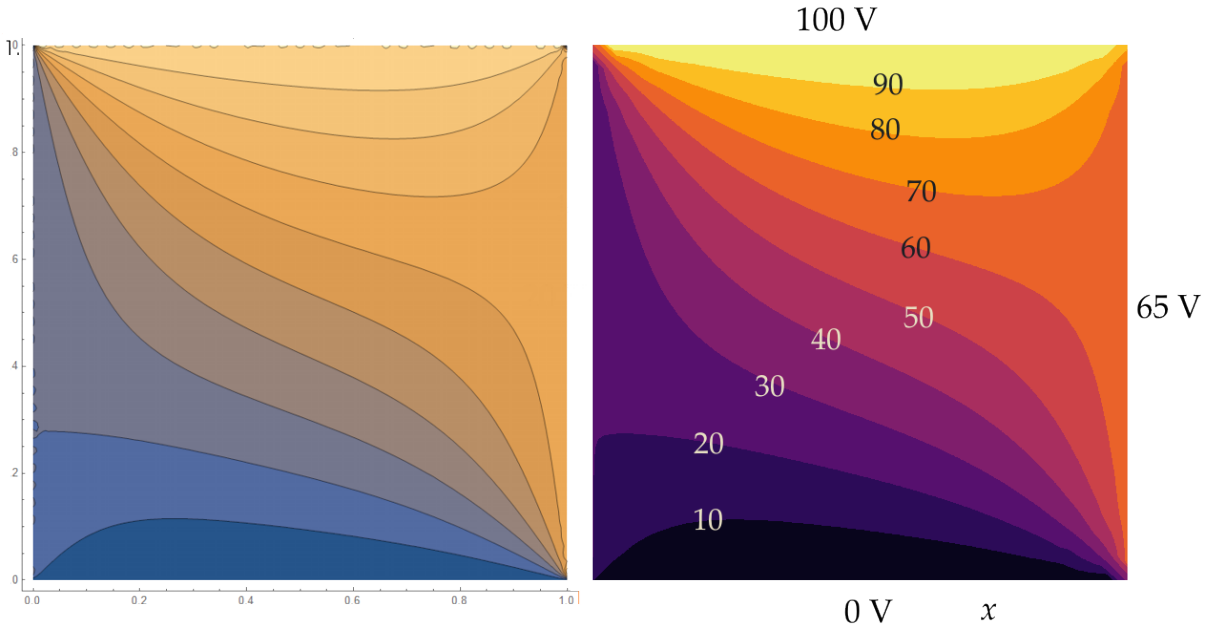

Figure 6: Contour plot of potentials for a general case in which all four sides are at different constant potentials. Left: theory, Right: FEA.

to points $z = 0$ and 1 in the z half-plane. The Schwarz-Christoffel formula is

$$\frac{dw}{dz} = Az^{-1}(z-1)^1, \qquad w = A\int_0^z \left(1-\frac{1}{z}\right) dz = A(z-\ln z) + C$$

where C is a constant of integration. To determine the constants A and C put in some values for z. At $z = 0$, $w = -A\ln(0) + C \to \infty$, meaning that this is the right hand ends of the two plates as they converge as $w \to \infty$. At $z = -1$, $w = A(-1 - i\pi) + C$ which is on the real w axis. Therefore $iA\pi + C = 0$, giving $C = iA\pi$. At $z = +1$, $w = B + ih$ for some B. Therefore

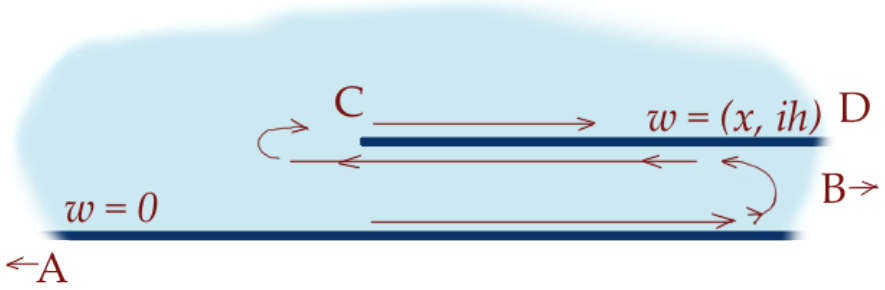

Figure 7: Semi-infinite plate parallel to an infinite plate in w-space. The path denoted by arrows is mapped to the upper half plane in z-space with B mapping to $z = 0$, C to $z = 1$.

$B + ih = A(1 + 0) + iA\pi$, making $h = A\pi$ or $A = h/\pi$. We arrive at

$$w = \frac{h}{\pi}(z - \ln z) + ih. \tag{7}$$

This places the left edge of the semi-infinite plate at $(h/\pi, ih)$.

The effect of the transformation on a square mesh can be seen in Figure 8. This is the reverse map from the z upper half-plane to the physical w-space. A mesh of unit squares in the z-plane has been mapped to the geometry of Figure 7. The images of four selected points are shown. The sharp point at the right is really at infinity.

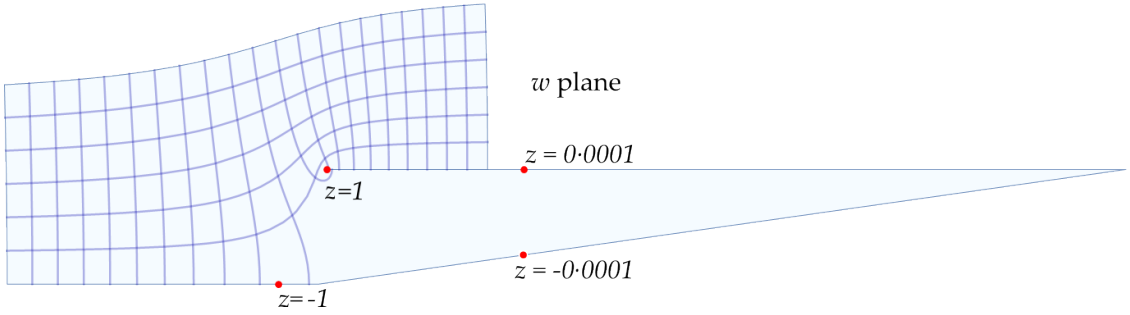

Figure 8: The conformal map of Eq 7.

The benefit of transforming to the upper half plane is that solutions to Laplace's equation are much more readily found there. The function $V = \ln z$, that is, $\ln(x + iy)$ satisfies $\partial^2 V/\partial x^2 + \partial^2 V/\partial y^2 = 0$. This can represent two conjugate arrangements:

1. a line of electric charge at the origin. The field lines are straight lines radiating from the origin and the equipotentials are concentric semi-circles centred on the origin as detailed in Appendix 1,

2. two or more conducting plates at different potentials radially arranged about the origin for which the field lines are semi-circles centred on the origin. In particular, two plates in line along the negative and positive real axis respectively with different voltages.

Here we use the second case. The field lines and equipotentials for the parallel plate geometry are obtained from these conjugate semi-circles and radial lines by the transformation of Eq

7. If $z = x + iy$, an equipotential is obtained by fixing the polar angle $\theta = \arctan(y/x)$ and letting $r = \sqrt{(x^2 + y^2)}$ increase from zero. The left panel of Figure 9 was obtained in this way. The voltage on the semi-infinite plate is π and the plotted equipotentials correspond to $\theta = 0,\ \pi/10,\ 2\pi/10,\ \ldots\ \pi$. This theoretical plot shows that, as seen from a large distance, the equipotentials appear to emanate from the mouth of the opening between the plates, making the field lines tend to semi-circles.

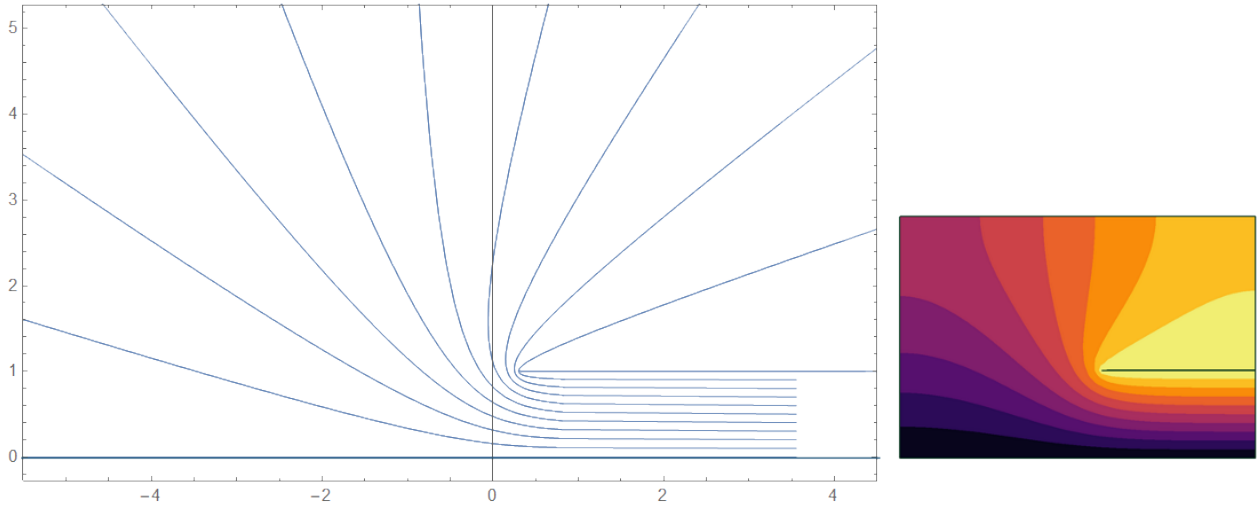

Figure 9: Equipotentials at $V/10$ intervals when semi-infinite plate is at potential V. Left: theory, Right: FEA.

The right panel in Figure 9 is the prediction of a finite element calculation of nominally the same geometry. Comparison of the two sets of curves shows a limitation of the FEA method. The material has been specified as an insulator with the properties of the vacuum. Note on the right how the equipotentials bend to be normal to the outer surfaces of the FEA mesh. This inability to deal well with fields as they tend to infinity is intrinsic in the FEA method. It occurs, for instance, with radiation of sound from a vibrating object; FEA manages the vibrating object itself well, but not the radiation. Some amelioration can be obtained by placing the region of interest in a large volume with a near-cylindrical or spherical shape as in Figure 10.

Case 2 : Fringe field of a parallel plate capacitor. If the field in Case 1 is mirrored about the infinite thin plate, and the voltage on the mirror semi-infinite plate changed from π to $-\pi$, we obtain a symmetrical geometry in which the central infinite plate lies on the equipotential which would exist between the two semi-infinite plates. This central infinite plate can therefore be removed without changing the field. The geometry has become the edges of two semi-infinite plates at different potentials. It was noted above that the function $V = \ln z$ describes the potential which satisfies Laplace's equation in each half space. Write $V = u + iv$ to obtain from Eq 7 parametric equations for the field in w-space:

$$w = \frac{h}{\pi}(e^V - V) + ih, \tag{8a}$$

$$w_r = \frac{h}{\pi}(e^u \cos v - u), \qquad w_i = \frac{h}{\pi}(e^u \sin v - v) + h \tag{8b}$$

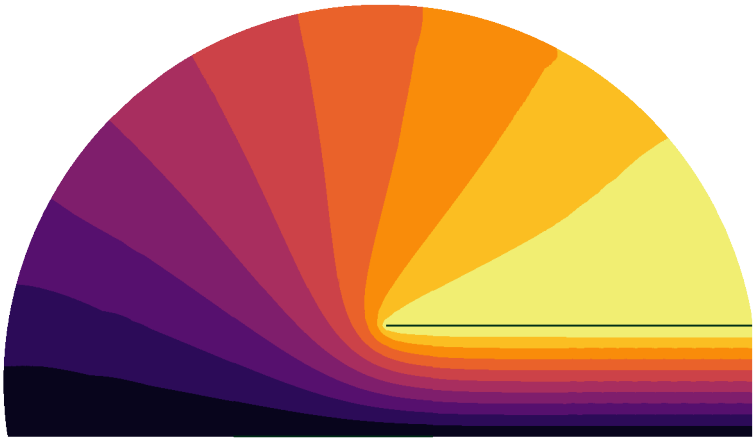

Figure 10: Revised FEA calculation of equipotentials as for Figures 7 and 9, attempting to improve accuracy at larger distances from the plate edge.

where w_r, w_i are the real and imaginary parts of the potential in w-space. This fringe field is illustrated in Figure 11.

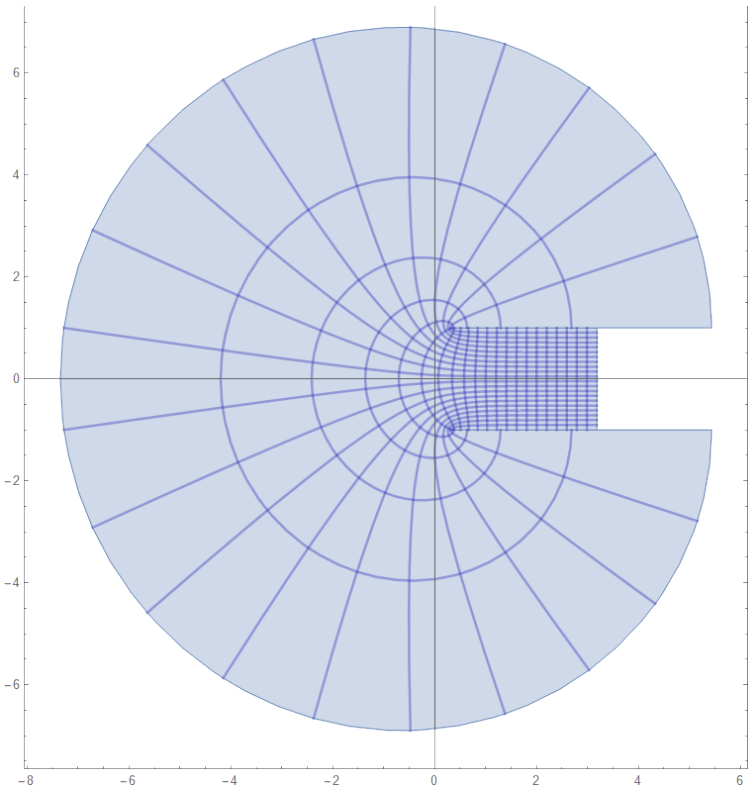

Figure 11: Equipotentials (radial) and field lines (circular) in fringe field of two semi-infinite plates at different potentials.

3.3 Fields in some other polygons

Having introduced the Scharz-Christoffel conformal transformation, we now discuss its application to other polygonal shapes for which the integration of Eq 6 is more challenging.

Case : Semi-infinite strip. Let the strip be parallel to the imaginary axis in physical w-space and extend a distance a either side of $\Re(w) = 0$. The two interior angles are each $\pi/2$, and let us carry the symmetry into z-space by mapping $w = (-a, 0)$ to $z = (-1, 0)$ and $(a, 0)$ to $(1, 0)$. Eq 6 becomes

$$\frac{dw}{dz} = A(z+1)^{-1/2}(z-1)^{-1/2}.$$

The integral can be approached in more than one way. I seems reasonable to combine the two roots into $\sqrt{z^2-1}$. Integrating and setting the constants A and C to give the values above, we obtain

$$w = \frac{a}{\ln(-1)}[-2\ln(\sqrt{z^2-1}+z)] + a. \tag{9a}$$

There is choice with the values of $\ln(-1)$, the square root, and $\ln(\sqrt{z^2-1}+z)$ when its argument is negative because both the square root and the logarithm are multivalued functions. For $\Re z > 0$ the correct mapping is obtained by taking $\ln(-1) = i\pi$, the positive square root and the principal value of $\ln(\sqrt{z^2-1}+z)$. For $\Re z$ negative the opposite sign of the root is needed. The required formula is

$$w = \frac{2ia}{\pi}\ln(\,\mathrm{sgn}(\Re z)\,\sqrt{z^2-1}+z) + a, \qquad \Re z > 0. \tag{9b}$$

Figure 12 shows how a square grid in the upper z half-plane is mapped to the strip.

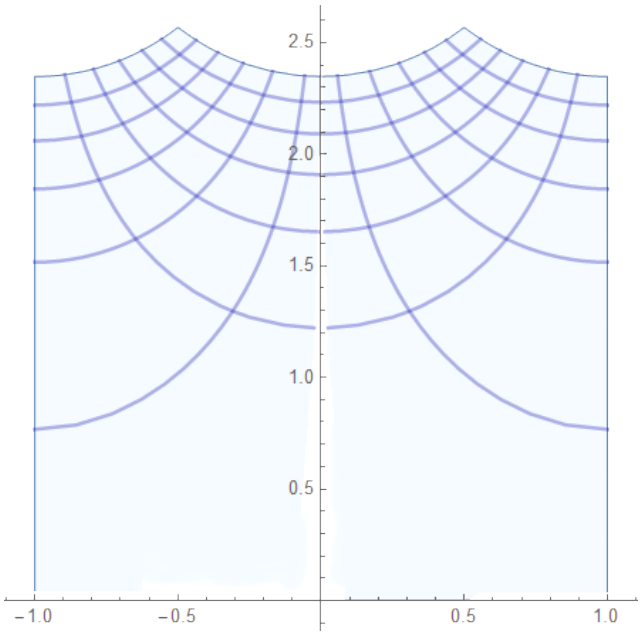

Figure 12: Mapping of z upper half-plane onto vertical strip of width 2 ($a = 1$) in w-space.

If the three sides of the strip are conducting planes, three simple ways to assign different voltages to them are

1. negative z section of boundary is at 0 V, positive at 100 V,
2. left vertical side at 0V, horizontal bottom and right side at 100 V,
3. left and right sides at 0 V, horizontal bottom at 100 V.

For arrangements 1 and 2 the voltage in z-space is $A \ln z$ as for §3.2, Case 1. Arrangement 3 requires the conjugate of two line sources at $z = \pm a$, namely $\ln(z \mp a)$.

4 Solutions of Laplace's equation in cylindrical co-ordinates

4.1 Two coaxial cylinders: the einzel lens

This is the classic electron lens element, well studied by Heddle in his book. I have examined the potential distribution using finite elements and typical results are shown in Figure 13. The upper panel shows the vacuum space inside the cylinders and their gap, and the lower panel the voltage contours. The equipotentials look almost circular in section, spherical in 3-D, with increasing radii near the cross-section of symmetry. The pattern will alter a little as the gap between the cylinders is changed, and will also be different if one cylinder has a larger internal diameter than the other. Where the diameters are the same, the field will be symmetric about the central (r, θ) plane of the gap and so can be split into its two halves about this plane. In the limit of vanishingly small gap the field is similar to the rectangular box in Figure 3.

This is a two-dimensional problem in cylindrical coordinates, with variables r radially and z along the axis. Where there is no dependence on the angle θ about the z axis, Laplace's equation is

$$\frac{\partial^2 V}{\partial r^2} + \frac{1}{r}\frac{\partial V}{\partial r} + \frac{\partial^2 V}{\partial z^2} \;=\; 0. \tag{10}$$

Using the separatin of variables device V can be shown to be the product of two functions, $R(r)$ and $Z(z)$ each depending on only one variable:

$$\frac{1}{R}\frac{\partial^2 R}{\partial r^2} + \frac{1}{rR}\frac{\partial R}{\partial r} + \frac{1}{Z}\frac{\partial^2 Z}{\partial z^2} \;=\; 0.$$

The sum of two completely independent functions of different variables can only be zero if each is a constant, σ^2, say, which could be complex. Hence

$$\frac{\partial^2 R}{\partial r^2} + \frac{1}{r}\frac{\partial R}{\partial r} + \sigma^2 R = 0 \qquad \text{and} \qquad \frac{\partial^2 Z}{\partial z^2} - \sigma^2 Z = 0.$$

The solution for Z is

$$Z(z) \;=\; C_1 e^{\sigma z} + C_2 e^{-\sigma z} \tag{11a}$$

while the solution for R involves Bessel functions:

$$R(r) \;=\; D_1 J_0(\sigma r) + D_2 Y_0(\sigma r). \tag{11b}$$

These Bessel functions have order 0 because the geometry is axisymmetric.

In principle such problems can be solved analytically by the analogue of Fourier series called Fourier-Bessel series. Taking only the left hand cylinder from Figure 13, and assuming radius a and length from $z = 0$ to L, the boundary conditions are:

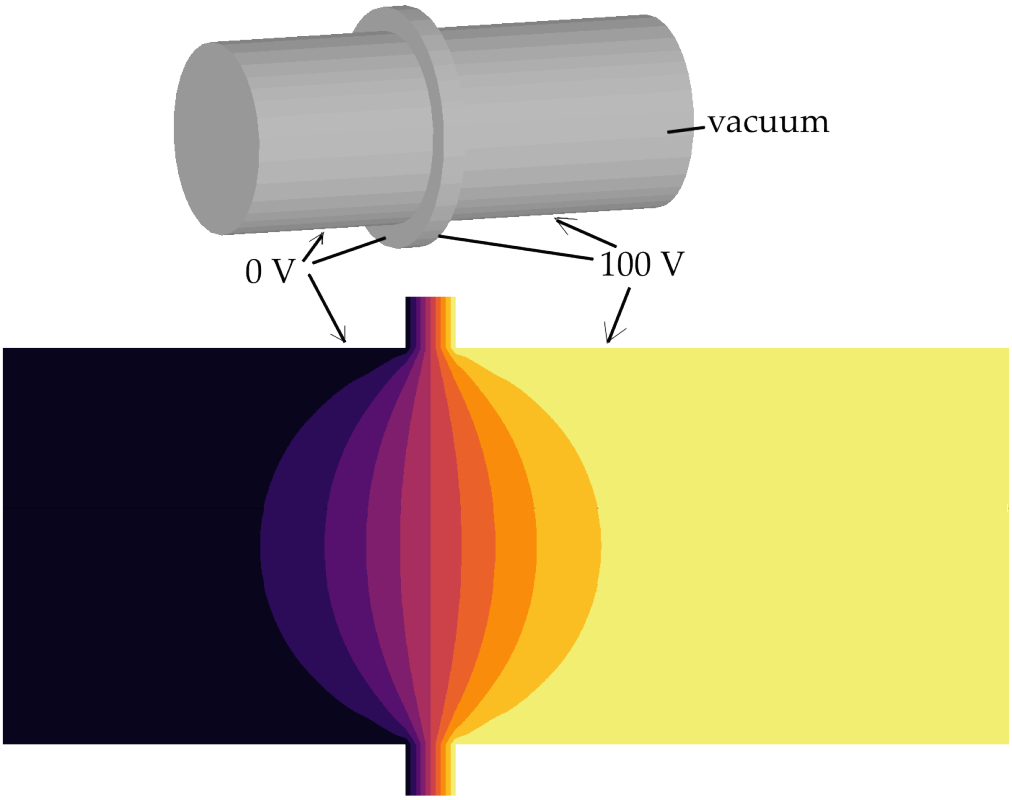

Figure 13: Top: FEA model of space between two in-line hollow conducting cylinders at potentials 0 V and 100 V. Bottom: potential distribution in the radial plane. Gap is 1/8th of internal diameter.

- $V = 0$ at $r = a$ for $z \neq 0$, $z \neq L$,
- $V = 0$ at $z = 0$,
- $V = V_0$ at $x = L$.

Because $V = 0$ at $z = 0$, the z dependence can involve only $\sinh(\sigma_k z)$ and not cosh functions, as we found at Eq 4. Radially, there can be no terms in Y_0 because this is infinite at $r = 0$.

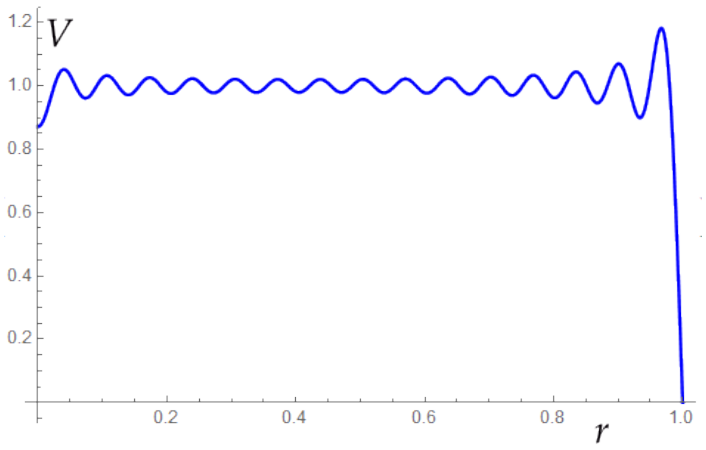

Figure 14: Bessel series approximation to unity over $r = 0$ to 1, by summing Eq 12 to 30 terms.

Therefore

$$V(r,z) \;=\; \sum_{k=1}^{\infty} D_k J_0(\sigma_k r)\sinh(\sigma_k z). \tag{12a}$$

To obtain $V = 0$ at $r = a$ we need $J_0(\sigma a) = 0$. The zeroes of $J_0(u)$ are tabulated and the first few are

$$u = \; 2\cdot 4048, \quad 5\cdot 5201, \quad 8\cdot 6537, \quad 11\cdot 7915, \quad 14\cdot 9309.$$

At $z = L$ V_0 needs to be transformed into a sum of Bessel functions and the coefficients determined using the orthogonality of Bessel functions. The relevant formulae are

$$\int_0^a z J_j(\sigma_j z) J_k(\sigma_k z)\, dz = 0, \qquad \int_0^a z J_k^2(\sigma_k z)\, dz = \frac{a^2}{2} J_{k+1}^2(\sigma_k a) \quad \text{where all} \quad J_i(\sigma_i a) = 0. \tag{12}$$

where the σ_k are in the list of zeros.

$$V(r,L) \;=\; V_0 \;=\; \sum_{k=1}^{\infty} D_k J_0(\sigma_k r)\sinh(\sigma_k L). \tag{12b}$$

The coefficients D_k are retrieved from

$$D_k \sinh(\sigma_k L) \;=\; \frac{2V_0 \int_0^a r\, J_0(\sigma_k r) dr}{a^2 J_1^2(\sigma_k a)} \;=\; \frac{2V_0}{\sigma_k J_1(\sigma_k)} \tag{13}$$

if $a = 1$. Figure 14 plots this approximation to $V_0 = 1$ from summing 30 terms of the series.

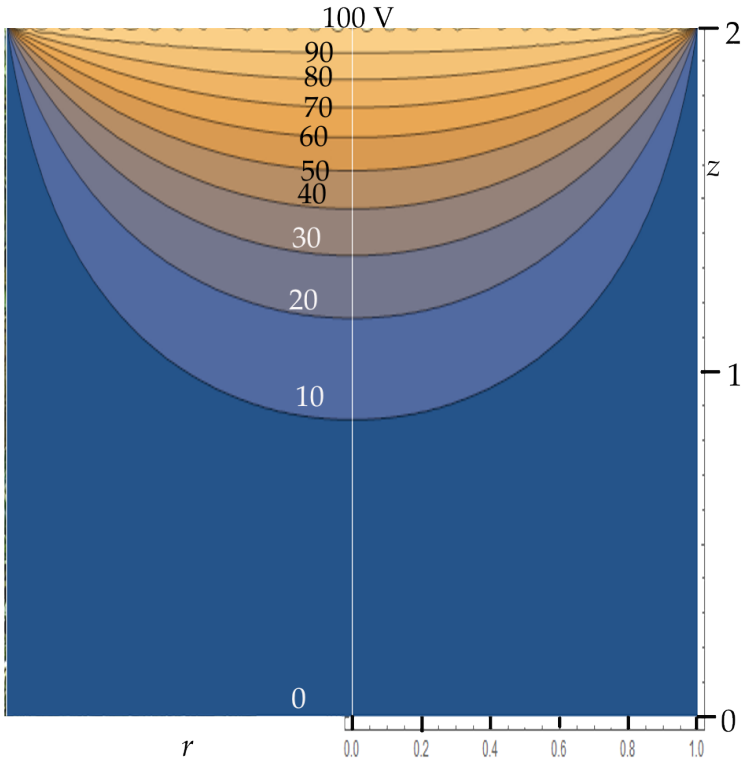

Figure 15: Contours of theoretical potential within hollow cylinder at 0V and 100 V at one cross-section. Radius 1, length 2.

The potential within the cylinder is

$$V(r,z) \;=\; 2V_0 \sum_{k=1}^{\infty} \frac{J_0(\sigma_k r)}{\sigma_k J_1(\sigma_k)} \frac{\sinh(\sigma_k z)}{\sinh(\sigma_k L)}. \qquad (14)$$

Contours of this are plotted in Figure 15 which can be compared with Figure 3 for a rectangular box and Figure 13 from FEA of two cylinders. I used Mathematica for this calculation and found it was quite slow.

It might be useful in practical calculations of electron deflection to have a set of simple formulae which give fair approximations to the potential near the z axis, that is, a paraxial approximation, without resort to tables of Bessel functions. This is less of an issue nowadays, but many years ago it was common for approximations to quantities involving 'special functions' to be published for other physicists to use. I have found that each contour of constant voltage in the (r,z) plane is close to a parabola for r up to $0{\cdot}4$ of the radius. Thus $z = c_0 + c_2 r^2$ on each contour. The variation of the coefficients with voltage over the left-hand cylinder are plotted in Figure 16. In this V is the fraction of V_0, the potential at the centre of the gap, and the cylinder is positioned in the left half plane from $z \to -\infty$ to $z = 0$, with $V \to 0$ as $z \to -\infty$. The contours are symmetric in shape in the right half plane of the other cylinder of the pair, with voltages correspondingly above V_0 and the right cylinder itself at $2V_0$. The

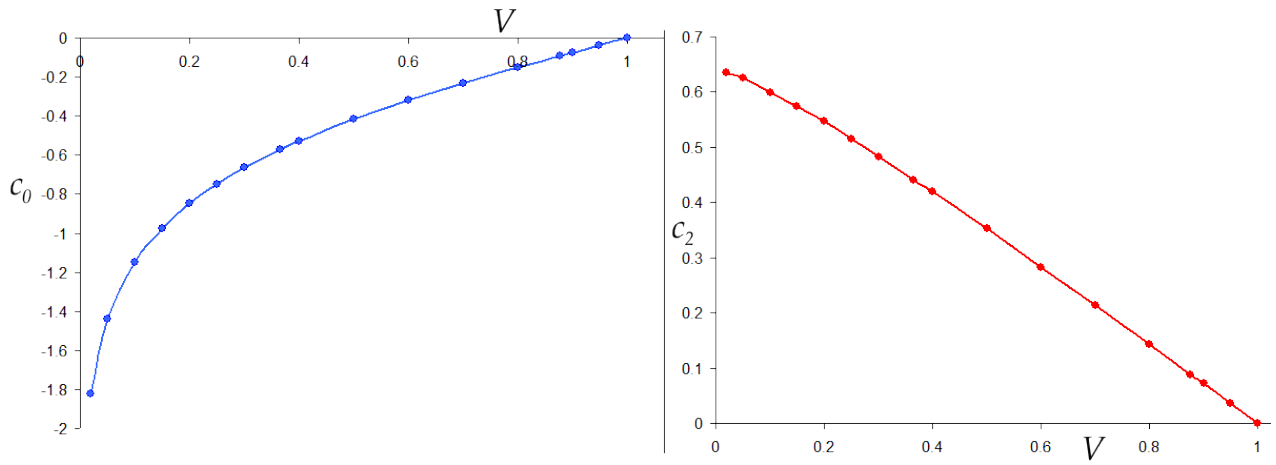

Figure 16: Coefficients of parabolas which approximate the contour plots for half of two adjacent hollow cylinders at different voltages. Left: c_0. Right c_2 in $z = c_0 + c_2 r^2$.

two coefficients can be approximated by fairly simple functions. The constant term depends almost logarithmically on V and can be made to fit well by adding a quadratic:

$$c_0 \;=\; a\ln(V) + b + cV + dV^2, \qquad a = 0{\cdot}41680,\; b = -0{\cdot}19517,\; c = 0{\cdot}07120,\; d = 0{\cdot}12397 \quad (15a)$$

which has been constructed so that $c_0 = 0$ at $V = 1$. c_0 is the axial position z at which voltage V occurs. Its inverse function is required for interpolation and is

$$V \approx Ae^{c_0} + B + Cc_0 + Dc_0^2 + Ec_0^3,$$

$$A = -4{\cdot}60737,\; B = 5{\cdot}60737,\; C = 6{\cdot}006,\; D = 2{\cdot}70785,\; E = 0{\cdot}47777. \qquad (15b)$$

The quadratic coefficient giving the off-axis potential varies almost linearly with V and is approximated by

$$c_2 = p + qV + sV^2, \qquad p = 0\cdot 65519,\ q = -0\cdot 55423,\ s = -0\cdot 10095. \tag{15c}$$

Using these formulae the potential at any position can be obtained as in the following example.

Example : Find the potential at $P = (r_0, z_0) = (0\cdot 37, -0\cdot 59)$.
Take $c_0 = z_0$. By Eq 15b the voltage on the axis here is $0\cdot 3543$ of that at the gap between the two cylinders. Following the contour from here to $r = r_0$, the contour moves closer to the gap by distance $c_2(V)r_0^2 = 0{\cdot}446r_0^2 = 0{\cdot}061$ (Eq 15c). Since adjacent contours stay almost the same distance apart with r, P will lie on a contour close to the one $0\cdot 061$ further away from the gap, that is, at $z_0 - 0\cdot 061 = -0\cdot 651$ where the voltage is $V = 0\cdot 3104$ according to Eq 15b. For some applications this may be a good enough approximation to the potential at P. The exact value from summing the Bessel series is $0\cdot 30506$. A second approximation can be obtained by finding a second contour, the one which has potential $0\cdot 3104$ on the axis. Using Eq 15a this is at $z = c_0 = -0\cdot 6511$. We follow this new contour out to r_0 and use Eq 15c to find $c_2 = 0\cdot 4735$, making the new $c_2r_0^2 = 0\cdot 0648$, larger than the previous $c_2r_0^2$. Call their difference ε. We therefore move in z from the second contour by ε to bring us closer to P. This puts us on a third contour which passes through the axis $r = 0$ at $z = -0\cdot 6548$. Eq 15c yields the voltage on this contour to be $0\cdot 3078$, which compares well with the Bessel series value of $0\cdot 30506$. From the point of view of beam focusing, the potential difference between axis and r_0 is perhaps more important than the absolute potential. The value $V(0, -0.59) - V(0.37, -0.59)$ is $0\cdot 0462$ by the Bessel series and $0\cdot 0465$ by the approximation method.

Table 2 lists points to compare summing the Bessel series with and the fitted curves. The percentage error with the approximation is highest where the field is weakest, at large distances from the gap and from the axis.

Extracting potentials from the FEA requires interpolation amongst the mesh nodes. I ran Mecway for the model in Figure 13 with the gap reduced to 5% of the radius. After

r	z	V_{Bessel}	V_{approx}	ΔV_{Bessel}	ΔV_{approx}
0.1	-0.1	0.867	0.863	0.001	0.001
0.2	-0.2	0.732	0.729	0.009	0.010
0.3	-0.3	0.594	0.595	0.029	0.028
0	-0.4	0.517	0.519	0	0
0.25	-0.6	0.323	0.326	0.020	0.021
0.35	-0.8	0.191	0.188	0.031	0.033
0.4	-1	0.113	0.109	0.028	0.028
0.15	-1.2	0.085	0.084	0.003	0.002
0.4	-1.5	0.034	0.043	0.009	0.008
0.3	-1.8	0.018	0.013	0.003	0.009

Table 2: Comparison of electric potential values calculated by summing Bessel series and from the approximation scheme using fitted curves. ΔV denotes $V(0, z) - V(r, z)$.

selecting the radial plane and shifting and scaling to bring co-ordinates of the FEA model into line with the theoretical one, a search of the sorted data was required to select four nodes which form the smallest quadrilateral containing point P. These four points were in general position, not neatly at the corners of a rectangle, so the interpolation formula was fairly complicated. I used the form $a + br + cz + drz = V$, solved for the four coefficients, and substituted the co-ordinates P to find $V(P) = 0 \cdot 3062$. In summary we have obtained three close values by these three approaches:

$$\text{Bessel series} : 0 \cdot 30506, \qquad \text{fitted curves} : 0 \cdot 3078, \qquad \text{FEA} : 0 \cdot 3062.$$

4.2 Circular ring of charge

The electric field around a charged disc depends on whether it is made of insulating of conducting material. The next subsection treats the case of a circular insulator over which the charge density is prescribed to be uniform, an idealised version of rubbing a plastic disc with wool or silk. The companion case of a conducting disc is considered in §4.4. Both analyses use the result for a single ring of charge since a disc can be constructed from a sequence of concentric narrow rings. A uniform, continuous ring of similar charge is a conceptual object made of an infinitely thin conducting charged loop. The charges are held in place by a notional rigid framework of oppositely charged ions. Any real object will have two sides, the faces of a metal plate, and a test charge will be affected by the field which is determined by all the charges. On the metal plate we can therefore distinguish the charge density on each face, whereas the ring of charge is only an infinitely narrow loop which looks both to $-z$ and $+z$.

First we determine the on-axis field. The left panel in Figure 17 illustrates the geometry. The charge on the element of area at (ρ, ϕ) is $\rho\,\delta\rho\,\delta\phi\,\sigma$ where σ is the charge density per unit area and $\delta\rho$ the infinitesimal width of he loop. The potential this creates at P on the axis at distance z is $-\rho.\,\delta\rho.\,\delta\phi.\,\sigma/r$ where $r^2 = \rho^2 + z^2$. Integrating with respect to ϕ

$$V(0,z)\Big|_{ring-axis} = \frac{-2\pi\sigma\rho\ \delta\rho}{\sqrt{\rho^2+z^2}}. \tag{16}$$

At large distances z this approximates to $-2\pi\sigma\rho\ \delta\rho/z$. Now $2\pi\rho\,\delta\rho$ is the area of the ring so from a great distance it appears like a point charge $q = 2\pi\sigma\rho\ \delta\rho$.

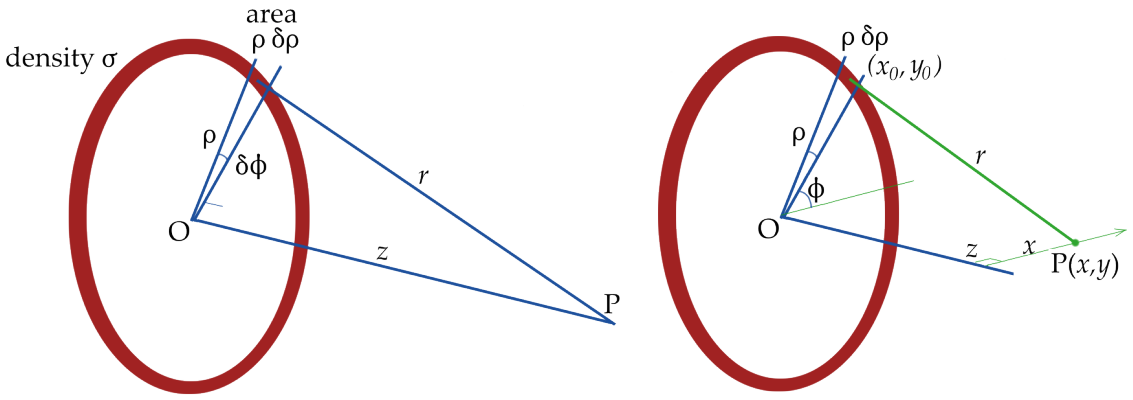

Figure 17: Potential of P due to a ring of charge. Left: on-axis geometry, right: off-axis.

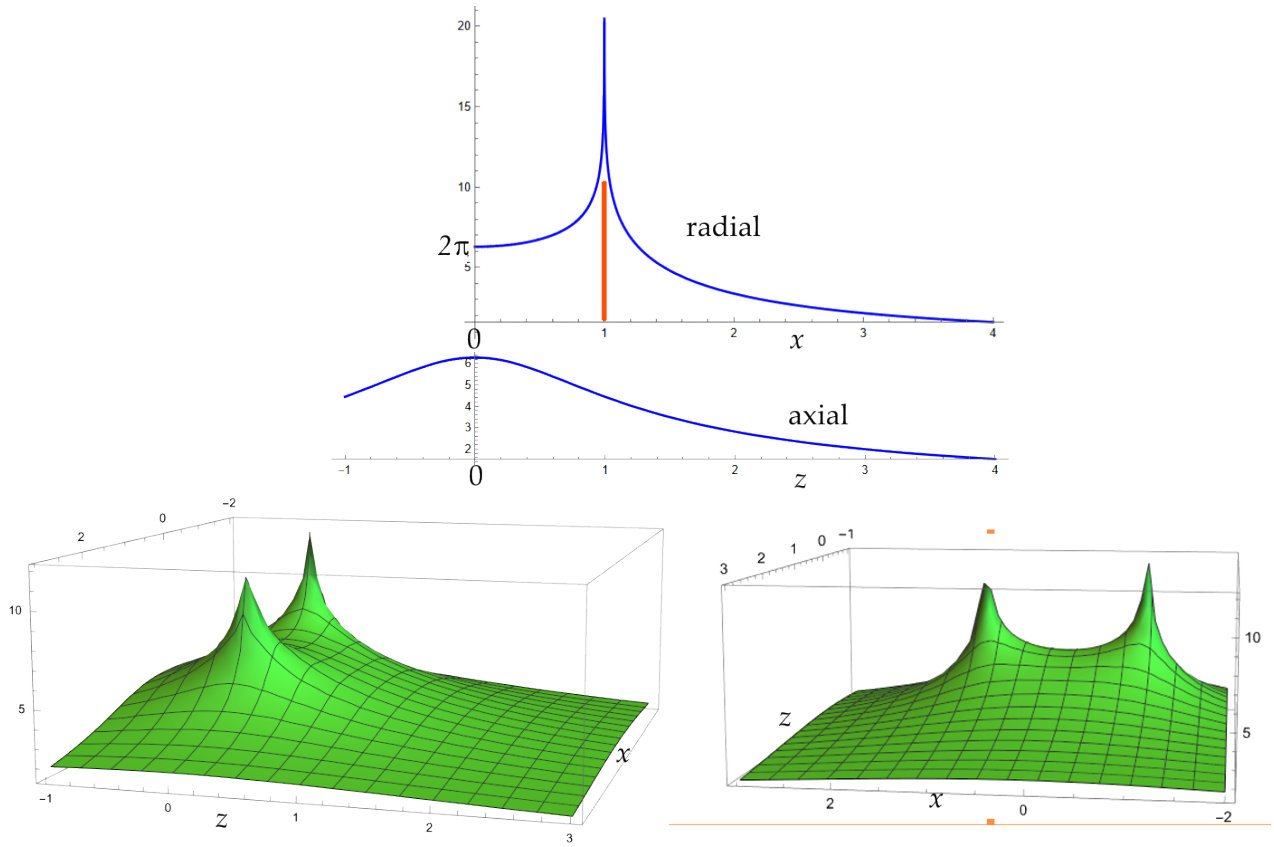

Figure 18: Four views of the electric potential around a circular ring of charge 1 unit in radius.

The field off-axis is found by reference to the right panel of Figure 17. The distance from the element of ring and the off-axis point $P(x, y)$ is

$$r^2 = (\rho\sin\phi)^2 + (x - \rho\cos\phi)^2 + z^2 = s^2 - 2\rho x\cos\phi \qquad \text{where} \quad s^2 = x^2 + \rho^2 + z^2.$$

The potential at P is therefore

$$V(x,z)\Big|_{ring} = -\sigma\,\rho\,\delta\rho\int_0^{2\pi}\frac{1}{r}\,d\phi = -\sigma\,\rho\,\delta\rho\int_0^{2\pi}\frac{1}{\sqrt{s^2 - 2\rho x\cos\phi}}\,d\phi. \tag{18}$$

This cannot be expressed in terms of elementary functions, but Appendix 1 Eq A1.2 shows that it can be converted to involve the 'complete elliptic integral of the first kind', $K(m)$, which is widely tabulated.

$$V(z)\Big|_{ring} = \frac{-4\sigma\rho.\delta\rho}{\sqrt{s^2 + 2\rho x}}\,K\left(\frac{4\rho x}{s^2 + 2\rho x}\right), \qquad K(m) = \int_0^{\pi/2}\frac{1}{1 - m\sin^2\alpha}\,d\alpha, \tag{19a}$$

$$s^2 + 2\rho x = (x + \rho)^2 + z^2.$$

The potential is illustrated in the four panels of Figure 18 for $\rho = 1$. The top panel shows the variation across a radius, $z = 0$, with the position of the ring marked by the red bar. Below is the axial variation, $x = 0$ out to 4 units. This gives a smooth saddle shape to the potential through the plane of the ring. The two 3D graphs are views of the potential across

any plane containing a diameter. Figure 19 complements these graphs with a contour plot over a radial-axial plane. As with a dipole, there is a contour (not shown) which intersects itself.

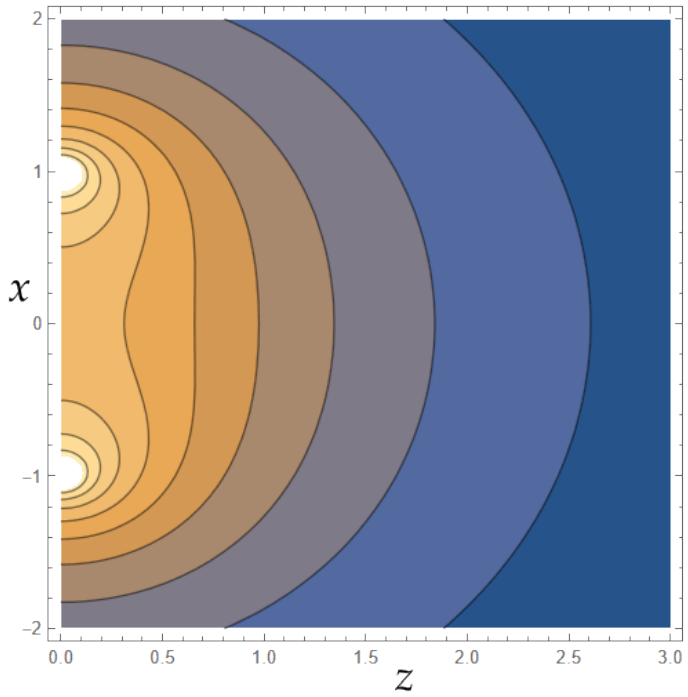

Figure 19: Contours of potential on a diametral section of a charged ring, unit radius.

Now consider the form of the singularity at the ring. The limiting form of $K(m)$ is given in Appendix 1, Eq A1.4. The ring can be approached in two directions of interest:

1. along a line parallel to the z axis, with x fixed at ρ and z approaching zero:

$$\frac{4\sigma\rho}{\sqrt{4\rho^2+z^2}}\,K\left(\frac{4\rho^2}{4\rho^2+z^2}\right) \;\to\; 6\ln 2 - 2\ln z \quad \text{for } \rho = 1, \tag{19b}$$

2. in the plane of the ring:

$$\frac{4\sigma\rho}{\rho+x}\,K\left(\frac{4\rho x}{(\rho+x)^2}\right) \;\to\; 6\ln 2 - 2\ln|1-x| \quad \text{for } \rho = 1. \tag{19c}$$

These show, as we might expect, that very close to the ring it appears like a line of charge whose potential falls logarithmically. The effects of curvature only appear away from the ring.

The electric field strength $\mathbf{E}(x,z)$ is the negative gradient of the potential. Close to the ring the $\ln r$ potential implies that $\mathbf{E}$ falls at $1/r$ in all directions. At larger distances we would need the vector gradient of Eq 18 which is everywhere normal to the equipotentials of Figure 19. Using the derivative of the elliptic function at Eq A1.5 in Appendix 1, in the plane of the ring the field is purely radial and given by

$$\mathbf{E}(x,0) \;=\; \frac{2\rho}{x}\left[\frac{E(u)}{\rho-x} - \frac{K(u)}{\rho+x}\right]\mathbf{e_x}\,, \qquad u = \frac{4\rho x}{(\rho+x)^2}\,. \tag{20}$$

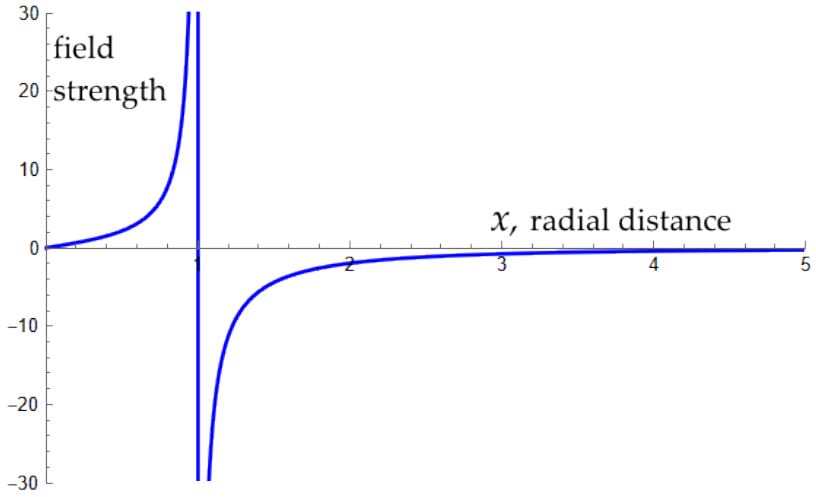

Figure 20: Electric field in plane of charged ring as a function of radial position. Radius 1.

Figure 20 plots this field strength in the plane of the ring from the centre at $x = 0$ out to $x = 5$. Although it falls to zero on the axis, the graph has a gradient of π/ρ^2, meaning that the force snaps from one radial direction to the opposite for a small displacement from the axis. In practice a free charged particle would accelerate either towards the ring or to a great distance in z depending on its sign.

4.3 Charged insulating disc

We picture the surface of the disc being constructed from concentric rings of charge. The on-axis field of a uniformly charged disc of insulating material, radius a, is found by integrating Eq 16, the on-axis potential of one ring, with respect to ρ. The integrand is the derivative of $\sqrt{\rho^2 + z^2}$ so

$$V(0,z)\Big|_{disc-axis} = -2\pi\sigma\left(\sqrt{z^2 + a^2} - z\right). \tag{21}$$

At large z this behaves as $-\pi a^2\sigma/z$; that is, as a point charge, Q = area × charge density.

At a general off-axis point P the calculation becomes more complicated. Referring to the right panel in Figure 17, by symmetry there is no loss of generality by taking the y co-ordinate of P to be zero.

$$r^2 = (x - x_0)^2 + y_0^2 + z^2 = (x - \rho\cos\phi)^2 + \rho^2\sin^2\phi + z^2.$$

The total potential at P due to one ring is

$$V(P)\Big|_{ring} = -\sigma\rho.\delta\rho\int_0^{2\pi}\frac{d\phi}{r(\phi)}.$$

In Appendix 1 I show how this can be transformed into an elliptic integral, a standard function whose values are tabulated and available in maths software packages. For small distances off-axis the Taylor series expansion of $1/r$ in powers of x gives a fair approximation. The potential

is symmetric about the z axis so only even powers of x contribute. The first three terms are

$$\rho \int_0^{2\pi} \frac{d\phi}{r(\phi)} \approx \frac{2\pi\rho}{\sqrt{\rho^2+z^2}} - \frac{\pi\rho\,(2z^2-\rho^2)}{2\,(\rho^2+z^2)^{5/2}}\,x^2 + \frac{3\pi\rho\,(8z^4-24\rho^2z^2+3\rho^4)}{32\,(\rho^2+z^2)^{9/2}}\,x^4. \qquad (22a)$$

Using Eq 18 and integrating over ρ, the near-axis potential of a uniformly charged circular disc, radius a, charge density $\sigma = 1$, is

$$V(P)\Big|_{disc} \approx -2\pi(\sqrt{z^2+a^2}-z) + \frac{\pi a^2}{2(z^2+a^2)^{3/2}}\,x^2 - \frac{3\pi a^2(4z^2-a^2)}{32(z^2+a^2)^{7/2}}\,x^4 + \ldots \qquad (22b)$$

This formula can be obtained either from Eq 18 or Eq 19a for the field of a ring of charge. The potential $|V|$ according to this approximation is plotted in Figure 18 for $a = 1$ unit, $x = 0$, $0\cdot2$, $0\cdot4$, $0\cdot6$. Note how the potential falls towards the rim of the disc; this is a consequence of its being made of insulating material. The curves show only slight variation with z even in the near-field.

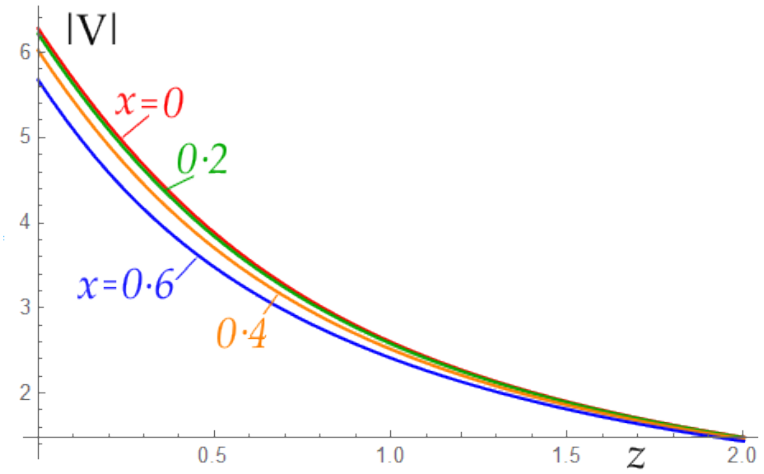

Figure 21: Axial and off-axis potential of a uniformly charged disc, unit radius, with distance z.

By comparison with numerical integration of the potential near the unit radius disc, I find that the series approximation to x^4 is generally accurate to better that $0\cdot5\%$, except towards the rim, as Table 3 below shows. Note that numerical integration has calculated the voltage at the the rim of the disc, $x = 1$, $z = 0$ to be exactly 4. Because the disc does not have a single surface potential, we cannot define a capacitance.

4.4 Charged metal disc

The more interesting but difficult case is where the disc is conducting. The charge density σ is not uniform but higher around the rim. The distribution of electric charge at the edge of an object is discussed more generally in the next section, §5. Here I quote how the disc is described in the book by Sir James Jeans[5]. He states that the 'density of electrification'

[5]The mathematical theory of electricity and magnetism', CUP, 5th edition 1925, p 248. Much the same analysis with similar notation is given by Sir Horace Lamb on pages 149 to 154 of his treatise on hydrodynamics. 6th ed. 1932, pub. Dover.

z	x	series	numerical
0	0	$2\pi = 6{\cdot}28319$	$6{\cdot}28319$
0	$0{\cdot}5$	$5{\cdot}87208$	$5{\cdot}86985$
$0{\cdot}2$	$0{\cdot}3$	$4{\cdot}61945$	$4{\cdot}61945$
$0{\cdot}4$	$0{\cdot}8$	$3{\cdot}42343$	$3{\cdot}44173$
0	1	$4{\cdot}418$	$4{\cdot}000$
1	0	$2{\cdot}60258$	$2{\cdot}60258$
1	1	$2{\cdot}12532$	$2{\cdot}12877$
$1{\cdot}2$	$0{\cdot}6$	$2{\cdot}13447$	$2{\cdot}13442$
2	1	$1{\cdot}35857$	$1{\cdot}35721$

Table 3: Potential $|V|$ of a uniformly charged unit disc calculated by series, Eq 22b, and numerical integration.

(on each face of the disc) is proportional to $a/\sqrt{a^2-\rho^2}$, a being the radius and ρ the distance from the centre, and so is essentially infinite at the rim. He proves that the capacitance of an isolated disc is $2a/\pi$, and further, that when the potential on the disc itself is 1, the potential at an external point (x, y, z) is

$$V \;=\; 2\pi \arctan\left(\frac{a}{\sqrt{\lambda}}\right) \qquad \text{where} \qquad \frac{z^2}{\lambda} + \frac{x^2+y^2}{a^2+\lambda} \;=\; 1, \quad \lambda \geq 0. \tag{23}$$

(The disc edge has $z = 0$, $x^2 + y^2 = a^2$ so $\lambda = 0$.) I can confirm that Eq 23 gives the same values as numerical integration of $a\rho/\sqrt{r^2(a^2-\rho^2)}$:

$$V(x,z)\Big|_{disc} \;=\; -\int_0^a \int_0^{2\pi} \frac{\sigma\rho}{\sqrt{r^2}}\, d\rho\, d\phi \;=\; -\int_0^a \int_0^{2\pi} \frac{a\rho}{\sqrt{(s^2 - 2\rho x\cos\phi)(a^2-\rho^2)}}\, d\rho\, d\phi$$

$$=\; \int_0^a \frac{4a\rho}{\sqrt{\big((x+\rho)^2+z^2\big)(a^2-\rho^2)}}\, K\left(\frac{4\rho x}{(x+\rho)^2+z^2}\right)\, d\rho. \tag{24}$$

The potential in a quadrant around a unit radius conducting disc is shown in Figure 22. The value on the disc is $a\pi^2$. As plotted in the right panel, it remains constant up to the edge of the disc then falls rapidly. The left panel shows contours of potential in a quadrant of space. The total charge, shared between the two faces of the disc, is

$$\int_0^a 2\pi\rho \frac{a}{\sqrt{a^2-\rho^2}}\, d\rho \;=\; 2a^2\pi$$

so the capacitance is

$$C \;=\; \frac{2a^2\pi}{a\pi^2} \;=\; \frac{2a}{\pi}$$

as Jeans has already shown.

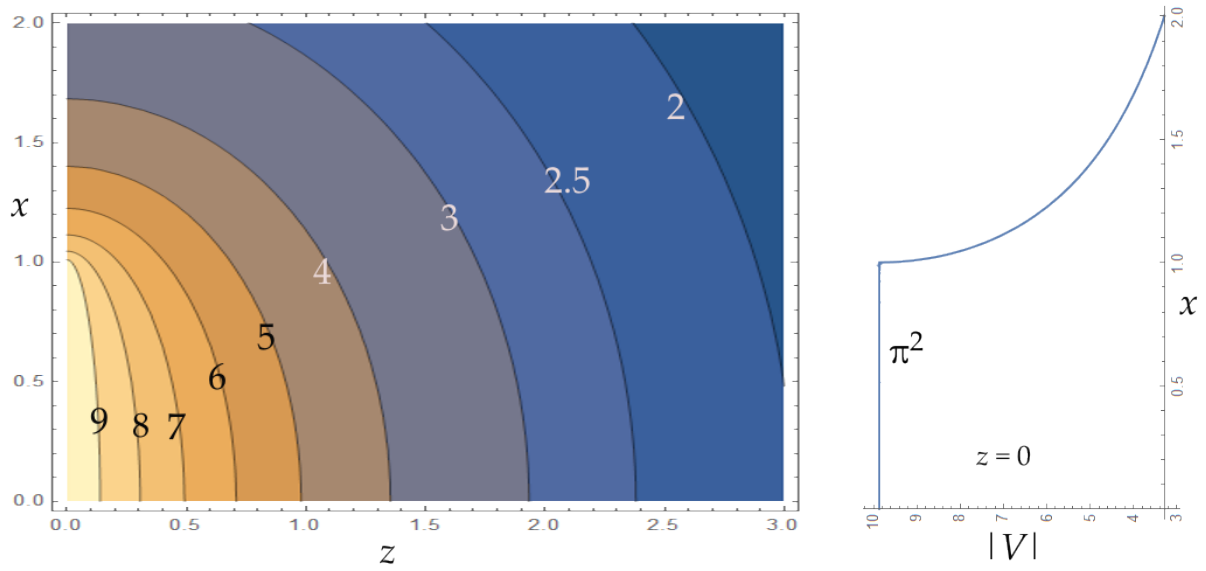

Figure 22: Potential $|V|$ on and around a charged conducting disc of unit radius.

5 Charge density over a conductor

Because charges on a conductor are free to move over its surface, the charge density over all but the most symmetrical objects varies with position. Calculations of potential outside and around the conductor require knowledge of this surface charge density distribution. This section discusses some simple cases.

5.1 Conducting disc and semi-infinite sheet

From §4.4 the formula $a/\sqrt{a^2-\rho^2}$ giving the charge density over a conducting disc has an intuitive interpretation. Figure 23 shows that $\sqrt{a^2-\rho^2}$ is the half-length of the chord at distance ρ from the centre. If we assume that the same amount of charge $2Q$ is contained in every strip between chords at ρ and $\rho+\delta\rho$, then the density at the diameter is Q/a and that at ρ is $Q/\sqrt{a^2-\rho^2}$. Thus $a/\sqrt{a^2-\rho^2}$ is the density at chord ρ relative to that at the diameter. It rises to infinity as the chord becomes rapidly shorter towards the edge.

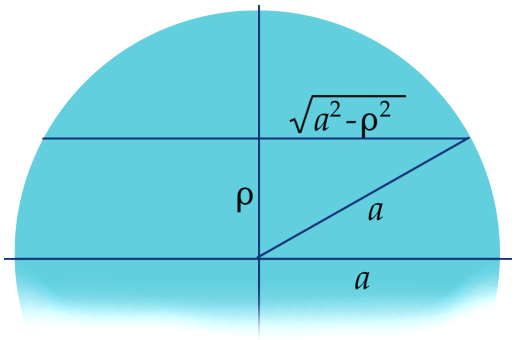

Figure 23: Intuitive explanation of increased charge density near edge of conducting disc, radius a.

On page 247 of his book Jeans derives Eq 23 and related formulae by analysing a conducting ellipsoid then collapsing its axes down to a disc. For the ellipsoid $x^2/a^2 + y^2/b^2 + z^2/c^2 = 1$ the construction for the charge density at any point on its surface is to draw the tangent plane at that point and calculate the perpendicular distance p from the centre of the ellipsoid to this tangent plane. The charge density is proportional to p where $p^2 = 1/(x^2/a^4 + y^2/b^4 + z^2/c^4)$. If c is very small,

$$p^2 \approx \frac{c^4}{z^2} = \frac{c^2}{\left(\frac{z^2}{c^2}\right)} = \frac{c^2}{1 - \frac{x^2}{a^2} - \frac{y^2}{b^2}}$$

so the charge density over an elliptical disc is proportional to

$$\frac{c}{\sqrt{1 - \frac{x^2}{a^2} - \frac{y^2}{b^2}}} \ . \tag{25}$$

A general point on the surface of the ellipsoid has been projected to a point in the plane of the elliptical disc. Morphing the ellipse to a disc gives the formula used above.

Taking the radius a of the disc to be very large and the position of interest to be near the edge, so $x = a - \epsilon$, $\epsilon << a$, we find the charge density near the edge varies as $\sqrt{a/(2\epsilon)}$. For large a, corresponding to an almost straight edge of a semi-infinite conducting plate, the charge density varies as $1/\sqrt{\epsilon}$. I here present an intuitive, heuristic account of why the charge density become large towards the edge of a conducting plate. Imagine an infinite sheet of metal with a straight line E drawn across it where a cut will soon be made. The crystal lattice of positively charged ion cores is surrounded by a 'gas' of thermally agitated mobile electrons in dynamic equilibrium, so there is no net migration of electrons. When the cut is made and the left half-plate removed, electrons near edge E no longer feel the repulsive force of mobile electrons to their left so are pushed leftwards by the electrons in the right half sheet, which try to expand away from one another. It is only the restraining attraction quantified by the work function of the material which prevents the electrons near E from being ejected leftwards from the plate.

Placing a conducting disc into an electric field, its surface is perpendicular to the field, is the complementary situation to placing a conducting plane with a circular hole perpendicular to the field, as discussed in §5.4. The first case is dealt with by Ferraro in his classic book on electromagnetism[6]. Like Jeans, he uses oblate spheroidal coordinates to determine the potential of an electrically earthed conducting spheroid aligned with its minor axis parallel to the field, then shrinks the spheroid to a disc. The field can be established between two distant, plane, parallel electrodes, one negatively charged, the other positively. Suppose the disc is first earthed so that it has no charge upon it, and then is insulated and introduced into the field. If it is placed at right angles to the field lines, its surface will correspond with an equipotential and, having no, charge it cannot disturb this potential. It therefore floats in voltage to the value at that position in the field. Charges will be induced on its left and right faces with signs opposite to those on the facing electrode so as to cancel the electric field inside the metal, but if the disc is thin, its perturbation of the applied field will be negligible.

[6] 'Electromagnetic Theory', V C A Ferraro, Athlone Press, 1954. p389.

Clearly the disc could be to connected to a battery to fix its potential at some value other than that of the field at that point. In that case the disc will have a net surface charge supplied by the battery and will disturb the applied field.

5.2 Conducting infinite strip

To quantify the redistribution of charge on the surface of an infinite flat metal strip, I have devised the following model. Consider a strip with parallel sides extending in width from E at $x = 0$ to E' at $x = 1$ and regard the mobile electrons as concentrated into discrete lines of charge parallel to E, E' as in Figure 24. We investigate the equilibrium positions of these lines. The force due to a line of charge falls as $1/r$ where r is the in-plane distance from the line. The force on any chosen line is the sum of the forces dues to all other lines. At equilibrium each of these is zero.

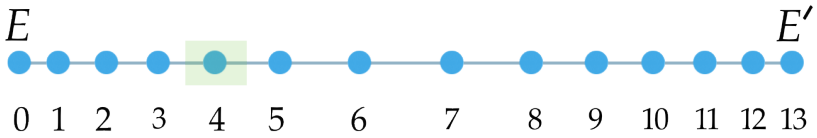

Figure 24: End-on view of 14 lines of charge across a strip with free edges E, E'.

Appendix 2 outlines the maths in this model and gives results for the equilibrium positions of N lines of charge for increasing N, obtained by numerical root-searching from approximate starting positions. The results predict that the line spacing will vary in an ellipsoidal way across the plate, with the largest spacing and hence lowest charge density at the mid-line of the strip, as we would expect from symmetry. Specifically, the graph of the length of strip δ_k occupied by line of charge k plotted against its position a_k is an ellipse. The green box around charge number 4 in Figure 24 shows the length δ_4 it is regarded as occupying. Figure 25 gives numerical results showing the ellipsoidal variation in δ_k for $N = 20$ and $N = 500$. (Figure 25 is identical to Figure 34 in Appendix 2.) The numbers prompt me to conjecture that in the limit the curve becomes

$$\frac{(x-0\cdot5)^2}{0\cdot5^2}+\frac{y^2}{\delta_{max}^2}=1 \quad \text{or} \quad \frac{\delta(x)^2}{\delta_{max}^2}=4x(1-x) \tag{26a}$$

where x is the distance from edge E and $\delta_{max} = \pi/(2N)$. The charge density σ is the reciprocal of δ so

$$\sigma(x) = \frac{N}{\pi\sqrt{x(1-x)}}. \tag{26b}$$

Here x and $1-x$ are distances from the nearest edge of the strip, so locally the charge density falls as $1/\sqrt{\epsilon}$, consistent with the result for an infinitely large disc found in §5.1. The integral of Eq 26b from $x = 0$ to 1 is N, as reqired.

Now that the charge density $\sigma(x)$ (per unit area) is known over the strip, the field at any point can be found numerically by integration over the potentials of line charges, which fall as $-\ln r$. Recall from §2 that the potential of a line charge with charge density σ per unit length is $-\kappa_C\pi\sigma\ln r$ where κ_C is Coulomb's constant and r the shortest distance from the line

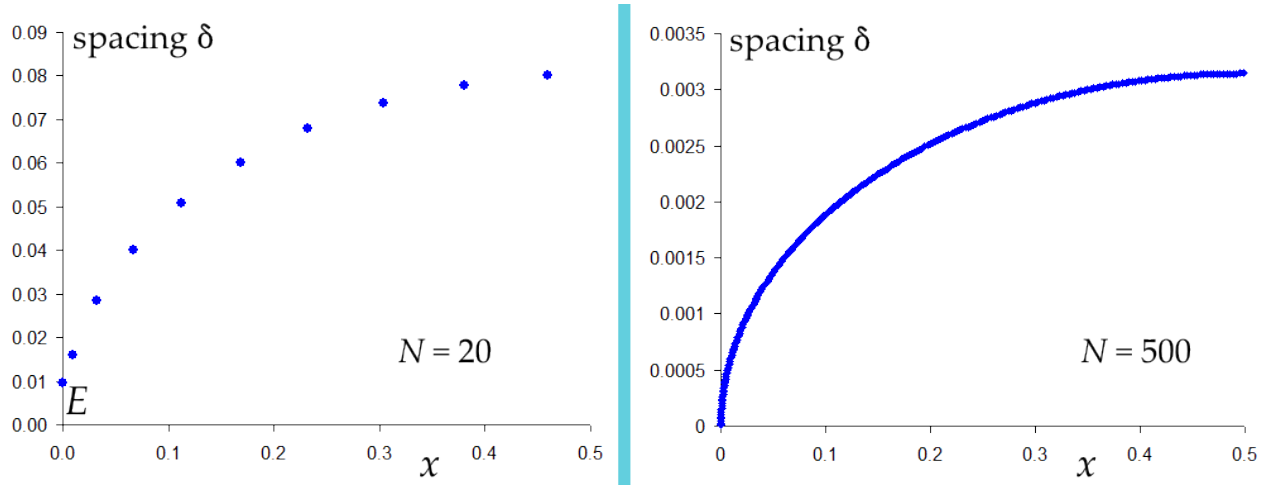

Figure 25: Spacing of 20 and 500 adjacent line charges across strip width 1, showing how their values fit around a quadrant of an ellipse. Strip edge E is at $x = 0$.

of charge to the point of measurement. Let (x, z) be a general point in space where z is the perpendicular distance from the strip, and let h be the distance from one end of the strip. The formula is

$$V_{strip}(x,z) \;=\; -\kappa_C \pi \int_{h=0}^{1} \ln(r(h))\sigma(h)\; dh \;=\; -\kappa_C \pi \int_{0}^{1} \ln(r)\, \frac{N}{\pi\sqrt{h(1-h)}}\; dh.$$

Taking $\kappa_C = 1$ for simplicity this is

$$V_{strip}(x,z) \;=\; -\frac{N}{2} \int_{0}^{1} \ln((x-h)^2 + z^2)\, \frac{1}{\sqrt{h(1-h)}}\; dh. \qquad (27)$$

N is the total charge per unit length (or area) of the strip and is shared between its two faces. As pointed out in §2, with a logarithmic fall in potential there is no natural position at which the potential it creates can be taken to be zero, so we have to select some position 'as zero'. For this figure I have let the integration in Eq 26 determine this for itself – it thus occurs about $0\cdot55$ units from the edge and sets the potential on the strip itself to be $\pi \ln 2 = 2\cdot1775$.

The potential is plotted in Figure 26 taking the total charge $N = 1$. In the left panel contours show the fall-off with distance in both z and x. In the right panel the potential across the strip itself is shown to be constant, confirming that the postulated charge density is correct. This graph has been rotated by 90° to align in x with the left panel.

It is now possible to calculate the potential distribution when the strip is charged and placed in an otherwise uniform electric field. In this example I will use arbitrary units of distance, potential, field strength, etc. rather than SI units. Suppose there are two large planar electrodes separated by 50 distance units and are at potentials 0 and 500 units respectively, so creating an electric field **E** of 10 units. Let the strip be charged by a battery to potential 30, then disconnected and placed in the field, parallel to the other two electrodes and half way

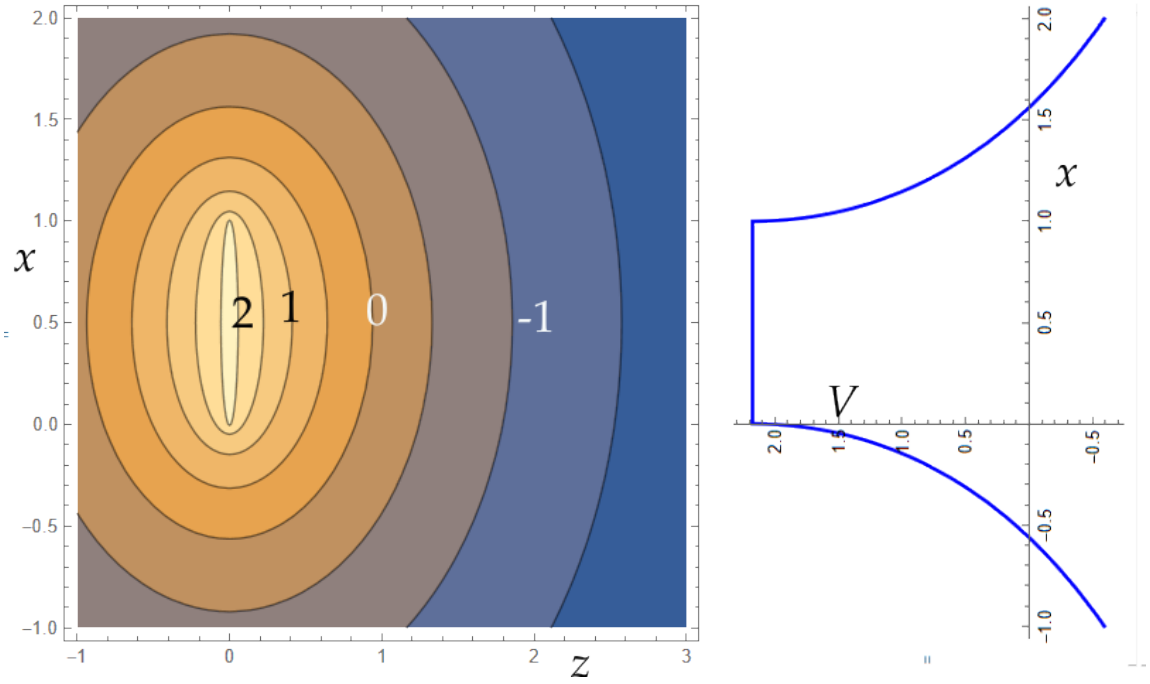

Figure 26: Potential on and around conducting strip between $x = 0$, $x = 1$.

between them where the potential would otherwise be 250. Because of the charge it carries, the strip will increase the potential locally by 30 to 280. The principle of superposition allows the potentials of two or more charge distributions to be added algebraically. It is necessary to specify the correct charge on the strip in order that its potential at $z = 0$ is 30 units greater than at $z = \pm 25$. Also the potential at $z = -25$ must be set to 0. From Eq 27 the combined potential is

$$V = (250 + 10z) + 20 \cdot 97 - 2 \cdot 074 \int_0^1 \frac{\ln \sqrt{(x-h)^2 + z^2)}}{\sqrt{h(1-h)}}\, dh. \tag{28}$$

The line plots in Figure 27 show the linear background potential in green and the perturbed potential through the middle of the strip at $h = 0 \cdot 5$ in blue. Figure 28 has contour plots of potential. Note the almost field-free space in the shadow of the strip. By Gauss's law the integral of the outwards electric fields over the surface will equal 4π times the enclosed charge, though I have not carried out this calculation to check. The reader may ask about the induced charges on the surface, positive on the left face, negative on the right. These are small. If the conductor is $0 \cdot 1$ units thick (much thicker than in practice), the potential difference in the external field will be only $10 \times 0 \cdot 1 = 1$ potential unit. The induced charges to cancel this will be equivalent to only $\pm 0 \cdot 5$ potential units on each face so I have disregarded them.

I cannot claim that these results for a strip are new, but I have not seen them in any textbook nor by a Google search.

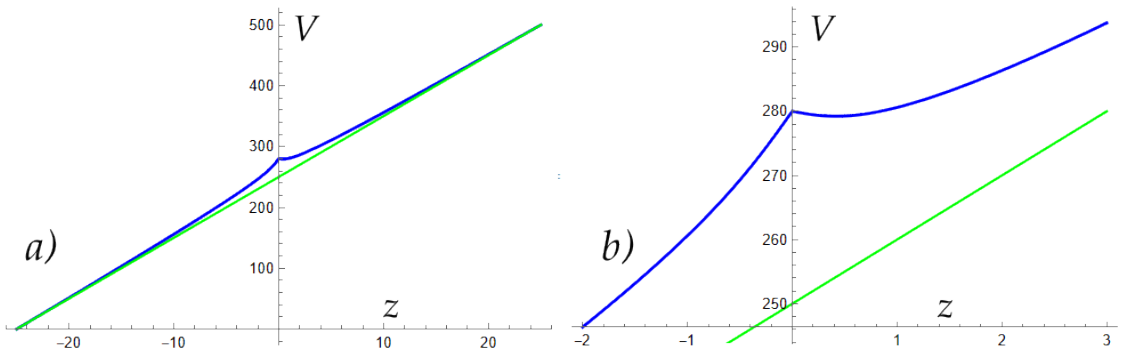

Figure 27: Potential through centre of strip, $x = 0 \cdot 5$, placed in uniform external field of 10 units. a): global view. b): details near strip at $z = 0$.

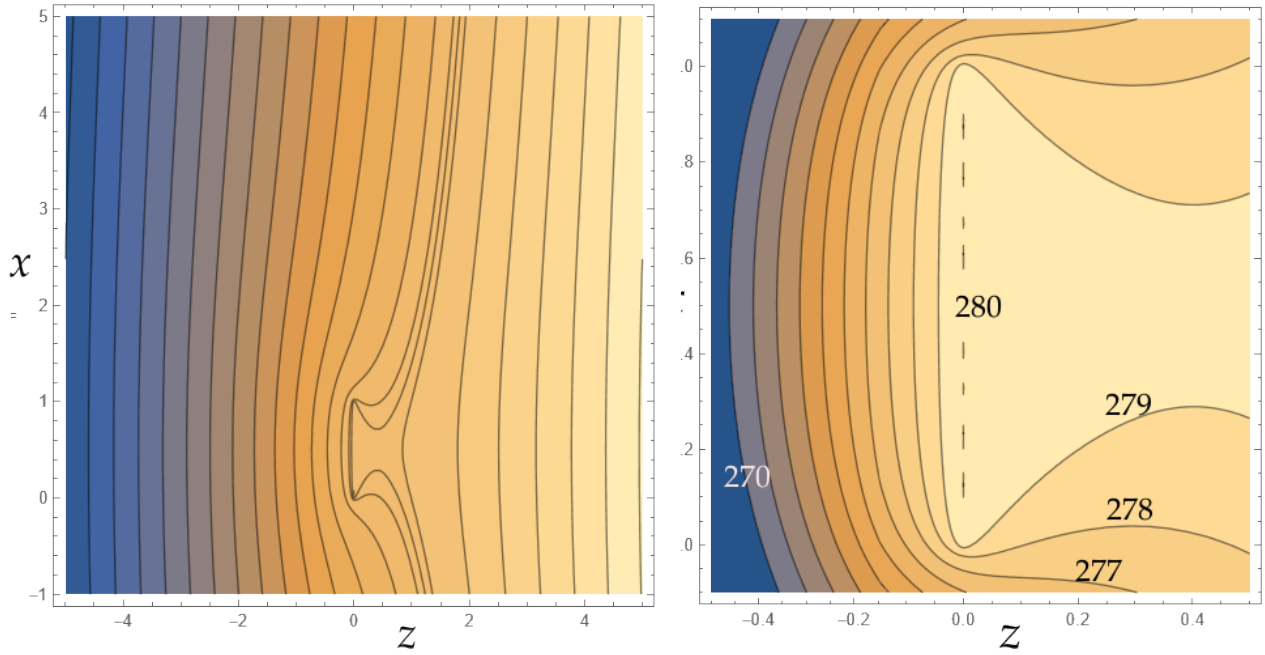

Figure 28: Equipotentials in the vicinity of the charged strip in an external field. Left: at 5 potential units separation. Right: at 1 unit separation near the strip, which extends from $x = 0$ to 1.

5.3 Charged conducting annulus

I have extended the method used in §5.2 in an attempt to obtain the charge density variation across a metal annulus. I had found nothing on this in the literature to which I have ready access until I had completed this work, when I found work done in 1949 by Higgins and D K Reitan[7], so it is possible that my results are new. Details are given in Appendix 3. Essentially we picture the annulus as being made of a set of concentric rings of the same type of charge, all constrained to the same plane, and with the inner one constrained to radius R and the outer to radius $R+1$. The rings between the inner and outer are allowed to expand or contract until the electric field at ring j, radius a_j, due to all the other rings is zero. This models the

[7] Thesis work published as 'Calculation of the capacitance of a circular annulus by the method of subareas', T J Higgins and D K Reitan, AIEE Trans. Vol 70, 1951, p926

ability of charge to flow over the annulus to equalise the potential.

The field strength due to one ring is given by Eq 20 of §4.2 and illustrated in Figure 20; it is repulsive in both the inwards and outwards directions. Because the field falls to zero more quickly inside the ring than outside, the outwards push from rings of smaller radius will exceed the inwards push of larger rings. Consequently, rings will be pushed up against the outermost one, giving a higher charge density at the outer rim than at the inner. In the limit of $R \to \infty$ the ring will look like a strip and the charge spacing should tend to the symmetrical ellipsoidal variation of Figure 25. The calculation follows that for the strip, though the mathematical functions describing the field are significantly more complicated.

The model has two parts:

1. a computer program to calculate the equilibrium positions, outputting a table of ring spacings at their equilibrium positions.
2. attempts at curve fitting to these tabular values to summarise the results and so allow ready calculation over a range of annulus shapes.

The fitted curve are fairly successful, since with them, over a wide range of R values, the potential across the annulus is found to be almost constant, which is the critical test of the model.

In Appendix 3 the fitting analytic curves to the tabulated data are hybrids between the two limiting forms of the curve at $R = 0$ and $R \to \infty$:

$$\sigma \;=\; \frac{Q_A\, J}{\pi^2 H\left(R+\frac{1}{2}\right)}, \qquad J \;=\; \sqrt{\frac{2hp-h-p}{h^3(1-5p)+8h^2p-3hp-h}}. \tag{29}$$

σ is the charge per unit area and H a scale factor to ensure that the total charge on the annulus is Q_A. This shape function $J(h,R)$ is an inelegant expression. I find J too opaque to give physical insight into the charge distribution, and it is almost certainly not the true analytic function, even though it should be useful for practical calculations should anyone wish to do them. The potential at a general external point is.

$$V(x,z) \;=\; \int_0^1 \frac{4\sigma(R+h)}{\sqrt{(x+R+h)^2+z^2}} K\left(\frac{4x(R+h)}{(R+h+x)^2+z^2}\right) dh\,. \tag{30}$$

Figure 29 is a contour plot of the potential in the radial-axial plane for $R = 1$. Note the closer equipotentials at the outer rim, a consequence of the higher charge density there. There is a saddle point at $(0,0)$ as with a simple ring.

I suspect that the true analytic functions describing the potential on and around an annulus are types of toroidal functions, since an annulus is a toroid which has collapses along its major axis. Solutions of Laplace's equation in toroidal coordinates have been described by William Hicks in a paper published in 1881[8]. In 1893 F Dyson published an article on

[8] W M Hicks, Phil Trans Royal Soc. Vol 172, p 609.

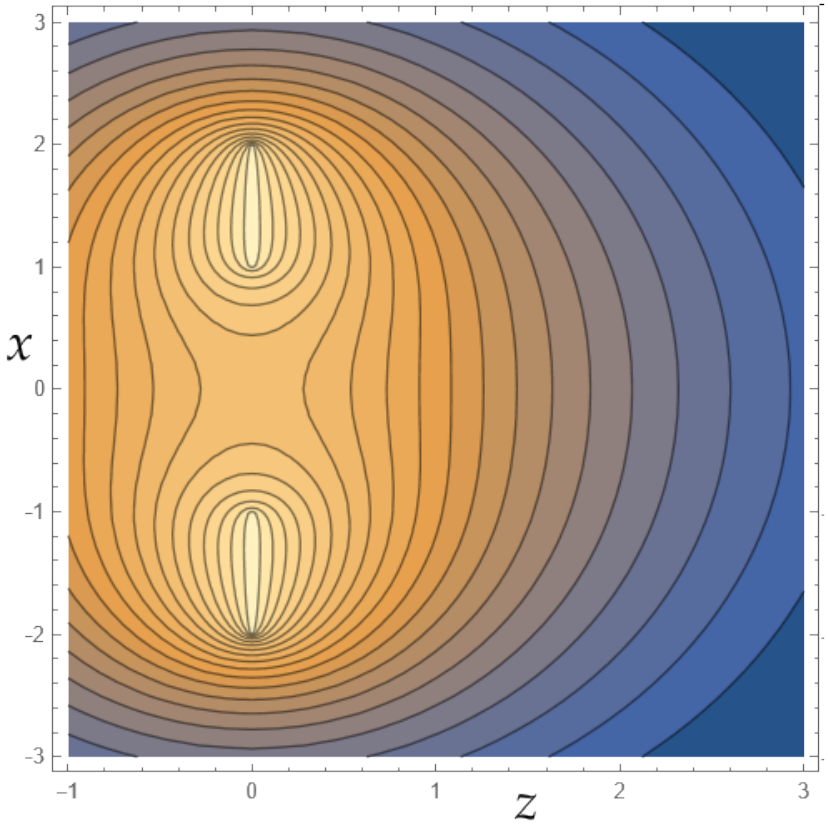

Figure 29: Contours of potential in the radial-axial plane of a charged conducting annulus with radii 1 and 2 units. z is axial direction.

the potential of an 'anchor ring'[9]. Dyson deals only with toroids whose minor sections are strictly circles, not ellipses, so they cannot be collapsed to an annulus, only to a single ring of charge. Much more recently Mark Andrews of Australia[10] has written on the application of toroidal coordinates to problems in electrostatics, inclining the field around a charged toroid. A paper on ellipsoidal toroidal coordinates with application to magnets for particle accelerators has been presented by Schnizer and colleagues[11]. Needless to say, toroidal coordinates, and especially elliptical ones, are complicated and arcane.

My model allows the capacitance C of an annulus between R and $R+1$ to be calculated. $C = Q_A/V$. I have calculated V at two positions across the metal and taken their average to produce the graph in Figure 30. When the central hole is small, the annulus behaves like a disc with capacitance $C = 2(R+1)/\pi$. The ratio C/C_{disc}, where the disc has radius $R+1$, remains essentially at 1 until $R \approx 0 \cdot 8$, and even at $R = 1$ is only $0 \cdot 98$. At larger radii the annulus starts to look like a single ring and, when large, C varies roughly as $0 \cdot 9R^{4/5}$.

[9] 'The Potential of an Anchor Ring'. F Dyson, Phil Tran Royal Soc London. A Vol 184, p43-95.

[10] 'Alternative separation of Laplace's equation in toroidal coordinates and its applications to electrostatics', M Andrews, J. Electrostatics, Vol 64, 2006, p 664.

[11] Cylindrical Circular and Elliptical, Toroidal Circular and Elliptical Multipoles Fields, Potentials and their Measurement for Accelerator Magnets', P and B Schnizer and E Fischer, found on-line via ReasearchGate, 2014

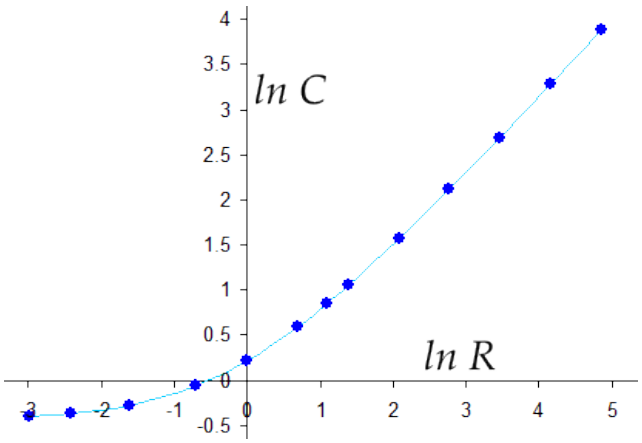

Figure 30: Log-log- plot of the capacitance of a conducting annulus with radii R, $R+1$.

5.4 Circular hole in a conducting plate

This is the simplest electron lens. It is constructed from three conducting planes parallel to each other and separated by distances d_1, d_2 so that the electric field in the left section is $\mathbf{E}_1$ and in the right is $\mathbf{E}_2$. A small circular hole is made in the central plate and so the stronger electric field protrudes a little through the hole into the space of the weaker field. The curved equipotentials around the aperture here will cause an incident electron beam to converge or diverge depending on its direction. The situation is illustrated in the two FEA contour plots in Figure 31.

The results in §5.3 above for the charged conducting annulus can go some way towards determining the potential at and around the aperture. It is necessary to select an annulus with a very small hole so that the metal approximates an infinite plate. The annulus is placed in a uniform electric field, as was the strip in §5.2. In the following numerical example I have chosen the inner radius R to be $0\cdot08$ units so that the width of metal is over 6 times the diameter of the holes. Even $0\cdot08$ is probably not small enough, but the model is perhaps less reliable for holes much smaller than this. I have used interpolated values from the tabular output of the computer program with 224 rings, instead of the more convenient but less accurate fitted curves. To calculate the charge density we also need $\sum^{224} a_j = 157\cdot72$.

The equipment is arranged as follows. The annulus is at $z = 0$ and the two large parallel planar electrodes are at ±10 distance units. At this distance the variation in x of the potential due to the annulus alone is almost zero. The electrodes have fixed potentials 0 and 500 so the background field $\mathbf{E} = 25$. We wish the annulus to have potential 100. Since the midway background potential is 250, the charge given to the annulus must be such that its potential is 250-100=150 units lower at $z = 0$ than at $z = \pm10$. The formula for the combined field is

$$V \;=\; (250+25z) \;+\; 10\cdot98 - 17\cdot65\int_{0\cdot08}^{1\cdot08} \frac{4\rho\sigma}{\sqrt{(x+\rho)^2+z^2}}\,K\left(\frac{4\rho x}{(x+\rho)^2+z^2}\right)d\rho,$$

where $\sigma = 1/(157\cdot72\,\delta)$ and $\delta(\rho)$ is the tabulated ring spacing for the 224 rings in the computer program.

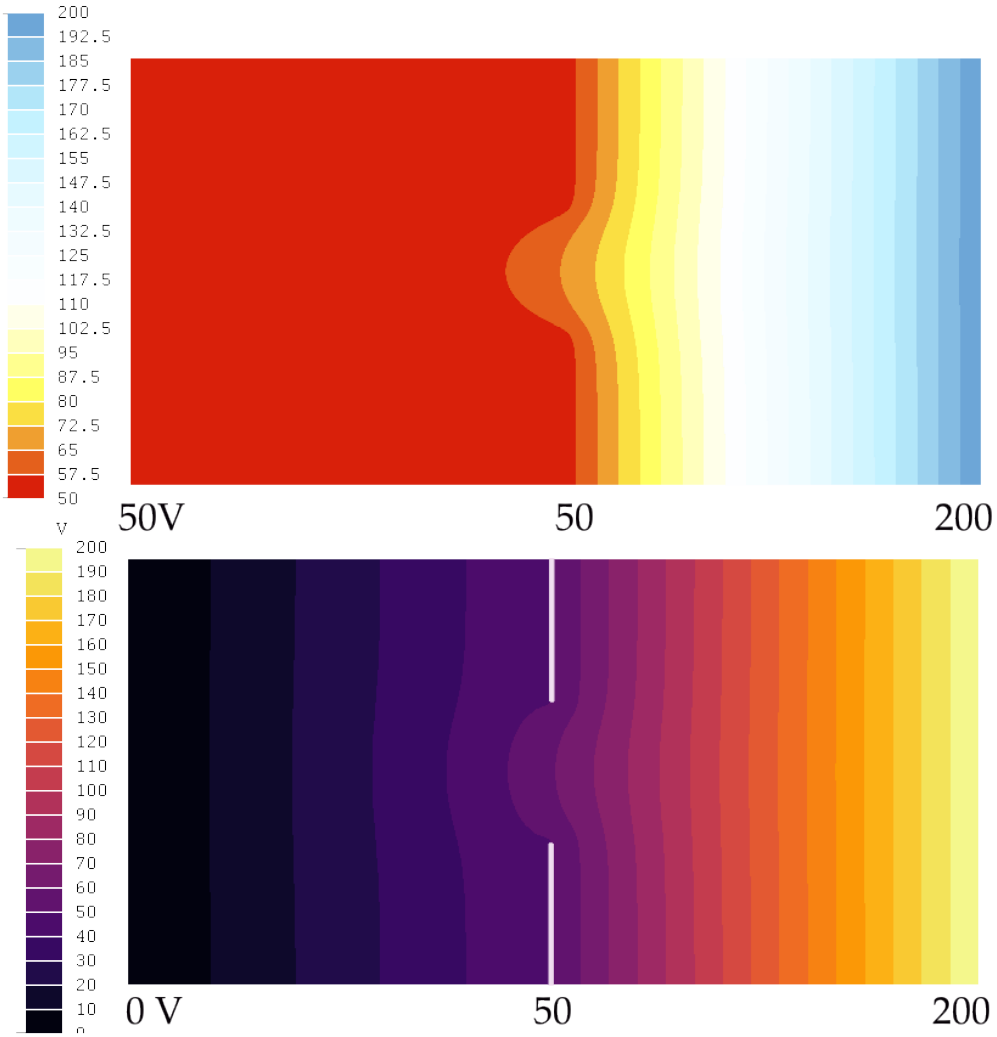

Figure 31: FEA values for the penetration of higher electric field into a weaker field through circular hole in a conducting plate. Top: voltages 50, 50, 200V, lower : 0, 50, 200V.

The results are disappointing. I had hoped that they would represent the field near the hole when the spaces either side have **E** of 10 units to the left and 40 to the right, but I have strong reservations regarding the outcome. Like the strip in §5.2, the annulus has pulled the voltage over itself up or down to the specified value, but has not changed the long range field. Therefore it is difficult to say what fields for $z < 0$ and $z > 0$ are being applied. The equipotentials at the hole are pinched into the hole a little. One might conceive of other schemes to give an improved representation, but I have decided not to pursue this further. The finite element solution is good.

I will conclude this article at this point and turn to other matters in Life.

Appendix 1: some simple systems

This appendix gives formulae for the electric fields and potentials of some simple configurations of charge.

Single line of electric charge

Figure 32 shows a uniform line of charge between a and b in the x direction, and a point charge P, strength q, at (c, z). The charge density in L is λ per unit length. The force between P and the element δx at x in the line is $f = \kappa_C\, q\, \lambda\, \delta x/((x-c)^2 + z^2)$ by Coulomb's law and is directed along the line between them.

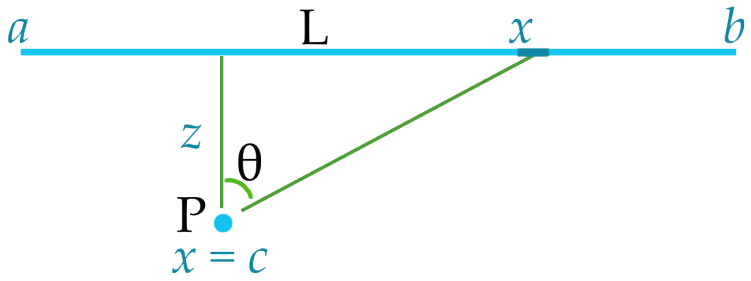

Figure 32: A point charge P near a uniform line of charge L.

Resolve f into components parallel and perpendicular to L and use $\cos\theta = z/\sqrt{(x-c)^2 + z^2}$:

$$f_\parallel = \frac{\kappa_C\, q\, \lambda\, (x-c)\, \delta x}{((x-c)^2 + z^2)^{3/2}}, \qquad f_\perp = \frac{\kappa_C\, q\, \lambda\, z\, \delta x}{((x-c)^2 + z^2)^{3/2}}.$$

Integrating with respect to x gives the force between L and P:

$$F_\parallel = \kappa_C\, \lambda q \left(\frac{1}{\sqrt{(a-c)^2 + z^2}} - \frac{1}{\sqrt{(b-c)^2 + z^2}} \right), \qquad F_\perp = \kappa_C\, \frac{\lambda q}{z} \left(\frac{c-a}{\sqrt{(a-c)^2 + z^2}} + \frac{b-c}{\sqrt{(b-c)^2 + z^2}} \right). \tag{A1.1}$$

Figure 33 plots these components for $\lambda = 1$, $q = 1$, $a = 0$, $b = 1$, $z = 0 \cdot 1$. When P is at the central position, there is no net parallel force and the perpendicular force for a line $2h$ long is

$$F = \frac{2\kappa_C\, h \lambda q}{z\sqrt{h^2 + z^2}}.$$

Of particular interest is the uniform infinite line of charge. Let $a = -b$, $c = 0$ and take the limit $b \to \infty$.

$$F \to \frac{2\kappa_C\, \lambda\, q}{z}. \tag{A1.2}$$

Since q can be regarded as a tiny test charge, the electric field strength of an infinite uniform line of charge is $2\kappa_C \lambda/z = \lambda/(2\pi\varepsilon_0\, z)$ where z is the distance from the line, and is directed perpendicular to the line. The potential is the integral of this: $V = 2\kappa_C \lambda \ln z + V_0$.

Looking at the potential further, we have in Eq A1.1 the components of the field **E** at any point P so the potential V in the space surrounding a finite line charge can be found by

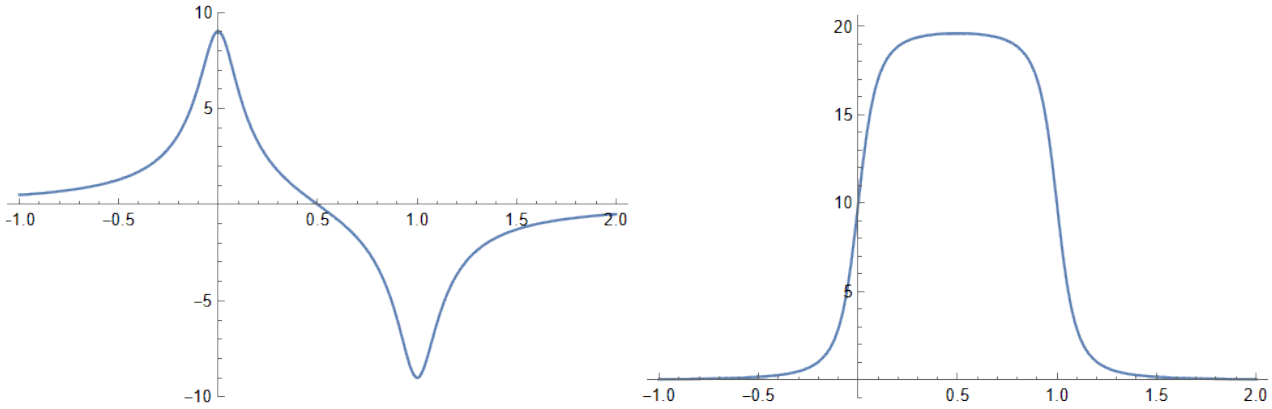

Figure 33: Components of force between line charge L and point charge P. Left: parallel to L. Right: perpendicular. Case $a = 0$, $b = 1$.

integration along a suitable path from a position of zero potential. We take the potential to be zero at infinity in both x and z, and follow any convenient path to the point P, integrating both components as we go as at Eq 2b. The integral to P is the scalar potential there. The line integral requires that we parametrise the path from infinite distance. For example, V in the mid plane is found by taking $a = -b$, $c = 0$ and letting z approach P in this central plane. Here $F_{\parallel} = 0$ by symmetry and

$$V_{mid\text{-}line} \;=\; \int_{\infty}^{z} \frac{2b\lambda}{z\sqrt{b^2+z^2}}\,dz \;=\; 2\lambda\ \mathrm{asinh}\left(\frac{b}{z}\right).$$

A further point: these calculations assume that the charge density remains uniform under all conditions and is not disturbed by forces from neighbouring charged objects. Such a line charge can only be on an insulating substrate over which charges have no capacity to migrate.

Two lines of electric charge

When there are two line charges, there are clearly many possible configurations – different lengths, separation and angles. I will deal only with two rod-like lines of uniform charge parallel to each other, though offset in position. The geometry is shown in Figure 34. The calculation can be done as a double integral over x_1 then x_2. We already have in Eq A1.1 the force of L_1 on an element of L_2 at x_2. Taking $\kappa_C = 1$ for convenience, the perpendicular force

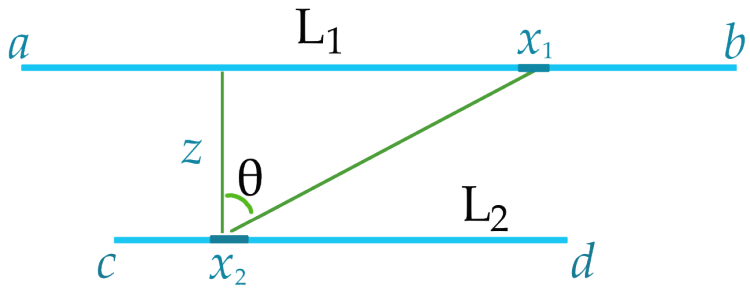

Figure 34: Two parallel uniform line charges in general position.

is

$$\mathcal{F}_\perp = \frac{\lambda_1 \lambda_2}{z}(AD - AC + BC - BD)$$

where $AC^2 = (a-c)^2 + z^2$, $AD^2 = (a-d)^2 + z^2$, $BC^2 = (b-c)^2 + z^2$, $BD^2 = (b-d)^2 + z^2$ and λ_1, λ_2 the respective charges per unit length. The parallel force is

$$\mathcal{F}_\parallel = \lambda_1 \lambda_2 [\ln(a-c+AC) - \ln(a-d+AD) - \ln(b-c+BC) + \ln(b-d+BD)].$$

Figure 35 plots both the parallel and perpendicular components for four sizes of the two lines as c increases and so moves one line past the other. In all cases $z = 1/10$, $\lambda_1 = \lambda_2 = 1$.

- Grey: $a = -1$, $b = 1$, $d = c + 1$,
- Blue: $a = 0$, $b = 1$, $d = c + 1$,
- Red: $a = 0$, $b = 1$, $d = c + 0 \cdot 5$,
- Green: $a = 0$, $b = 1$, $d = c + 0 \cdot 25$.

As the smaller rod gets shorter, the graphs tend towards those in Figure 33. When two lines each of length $2h$ are directly opposite each other with no off-set, the parallel force is zero (by symmetry) and the perpendicular force per unit length is

$$\frac{\lambda_1 \lambda_2 \left(2\sqrt{4h^2 + z^2} - 2\sqrt{z^2}\right)}{2hz}. \qquad (A1.3)$$

As h tends to infinity this attains the limiting value of $2\lambda_1 \lambda_2 / z$. This is simply the field strength of one line multiplied by the linear charge density of the other line.

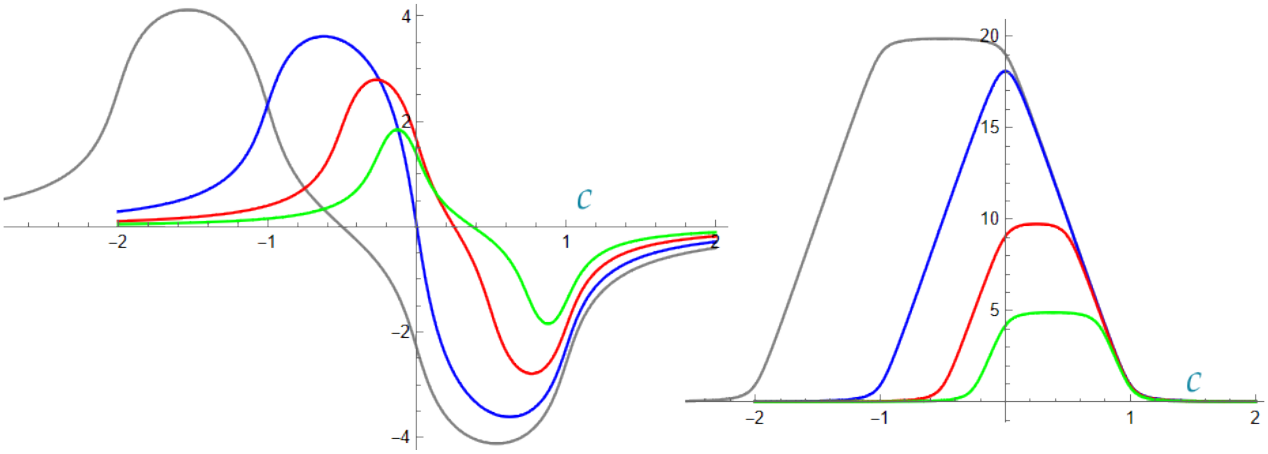

Figure 35: Components of force between two parallel line segments of uniform charge. Left: parallel. Right: perpendicular.

Ring of charge using elliptic integrals

This is a calculation of the potential at a general off-axis point $P(x,y)$ of both a ring and a disc of charge as in Figure 17. Referring to the right panel in the figure, the distance r from the element on the ring at (x_0,y_0) to P at $(x,0)$ is

$$r^2 \;=\; (x-x_0)^2 + y_0^2 + z^2 \;=\; (x-\rho\cos\phi)^2 + \rho^2\sin^2\phi + z^2 \;=\; s^2 - 2\rho x\cos\phi,$$

where $s^2 = x^2+\rho^2+z^2$. The potential at P due to all elements of a single ring is

$$V(z)\Big|_{ring} \;=\; -\sigma\rho.\delta\rho\int_0^{2\pi}\frac{d\phi}{r(\phi)}.$$

With some work this can be transformed into a standard elliptic integral in the notation of Abramowitz and Stegun's 'Handbook of Mathematical Functions',

$$F(\alpha,m) \;=\; \int_0^{\alpha}\frac{dx}{\sqrt{1-m\sin^2 x}}, \qquad 0<m<1, \quad F\left(\tfrac{\pi}{2}|m\right)\equiv K(m). \qquad (A1.4)$$

$F(\alpha,m)$ is an 'incomplete elliptic integral of the first kind', and with $\alpha=\pi/2$ becomes a 'complete elliptic integral of the first kind'.

The transformation is as follows. By the trigonometric formula $\cos\phi = 1-2\sin^2(\phi/2)$, and with $v=\phi/2$, the potential becomes

$$-2\sigma\rho.\delta\rho\int_0^{\pi}\frac{dv}{\sqrt{(s^2-2\rho x)+4\rho x\sin^2 v}} \;=\; \frac{-2\sigma\rho.\delta\rho}{\sqrt{s^2-2\rho x}}\int_0^{\pi}\frac{dv}{\sqrt{1+\frac{4\rho x}{s^2-2\rho x}\sin^2 v}}.$$

For P on the axis $x=0$ and the potential is that of Eq 16, §4.2. We note that $s^2-2\rho x>0$ for all values of x. It takes its minimum value of z^2 at $x=\rho$, which is positive for P not on the ring itself. Therefore the quantity $b^2 = 4\rho x/(s^2-2\rho x)$ is positive and the integral is not of the standard form A1.1. Therefore make the transformation $w=\pi/2-v$, so $\sin v=\cos w$ and $dv=-dw$.

$$1+b^2\cos^2 w \;=\; 1+b^2-b^2\sin^2 w \;=\; (1+b^2)\left(1-\frac{b^2}{1+b^2}\sin^2 w\right), \quad 1+b^2 \;=\; \frac{s^2+2\rho x}{s^2-2\rho x}.$$

$$V(z)\Big|_{ring} \;=\; \frac{-2\sigma\rho.\delta\rho}{\sqrt{s^2+2\rho x}}\int_{-\pi/2}^{\pi/2}\frac{dw}{\sqrt{1-m\sin^2 w}}, \qquad m=\frac{b^2}{1+b^2}=\frac{4\rho x}{s^2+2\rho x}.$$

$$V(z)\Big|_{ring} \;=\; \frac{-4\sigma\rho.\delta\rho}{\sqrt{s^2+2\rho x}}\,K(m)\,, \qquad s^2+2\rho x=(x+\rho)^2+z^2 \qquad (A1.5)$$

where use has been made of the symmetry $F(-\alpha|m)=-F(\alpha|m)$. This exact expression is to be compared with the series expansion Eq 18 in §4.2:

In the plane of the ring $z=0$ and $s^2\to x^2+\rho^2$ so the potential is

$$V(z)\Big|_{z=0} \;=\; \frac{-4\sigma\rho\,\delta\rho}{x+\rho}\,K\left(\frac{4\rho x}{(x+\rho)^2}\right) \qquad (A1.6)$$

$K(m)$ diverges to $+\infty$ at $m = 1$. Its asymptotic behaviour is found from expressions in the 'Handbook of Mathematical Functions' by Abramowitz and Stegun at 17.3.11, 17.3.17, 17.3.21. These show the relations between $K(\epsilon)$ and $K^\dagger(\epsilon) \equiv K(1-\epsilon)$ for $m = \epsilon << 1$. Near 0,

$$K(\epsilon) \approx \frac{\pi}{2}\left(1 + \frac{1}{4}\epsilon + \frac{9}{64}\epsilon^2 + ...\right)$$

A quantity called the 'Jacobian nome', q, is given by

$$q = g + 8g^2 + 84g^3 + 992g^4 + 12514g^5 + ... \qquad \text{where} \quad g = \frac{m}{16}$$

and has the property that

$$\frac{K^\dagger}{K} = -\frac{1}{\pi}\ln q.$$

Putting these series together

$$K(1-\epsilon) \equiv K^\dagger(\epsilon) \approx 2\ln 2 - \tfrac{1}{2}\ln\epsilon = 2\ln 2 + \ln\frac{1}{\sqrt{\epsilon}}. \qquad (A1.7)$$

This shows the potential near the ring, but we cannot speak of the potential on the ring itself.

Another approach to the potential close to the ring can be obtained from Gauss's theorem. Consider a short arc of the ring with length $\rho\,\delta\phi$ as in Figure 17. The charge inside is $\sigma\rho\,\delta\rho\,\delta\phi$. Consider also the ring to lie wholly inside a virtual toroid with a small sectional radius ε, so the toroid encloses the ring. The surface area of this toroid along the short arc is $2\pi\varepsilon\rho\,\delta\phi$. By Gauss's theorem the outwards flux of electric field $\mathbf{E}$ satisfies

$$2\pi\varepsilon\rho\,\delta\phi\,E = 4\pi\,\sigma\rho\,\delta\rho\,\delta\phi, \quad \text{so} \quad E = \frac{2\sigma}{\varepsilon}.$$

The potential is the integral of this, $2\sigma\ln\varepsilon$. This is not Eq A1.7, though the logarithmic fall-off is predicted.

The electric field strength and hence the force on a nearby charge are given by the gradient of the potential and for this we need the derivative of $K(m)$:

$$\frac{dK(m)}{dm} = \frac{1}{2m}\left[\frac{E(m)}{1-m} - K(m)\right] \qquad \text{where} \quad E(m) = \int_0^{\pi/2}\sqrt{1 - m\sin^2\theta}\,d\theta \qquad (A1.8)$$

is the well-tabulated 'complete elliptic integral of the second kind'.

Appendix 2: Conducting strip: equilibrium of line charges

This Appendix gives details of the model in §5.2. A strip of unit width is modelled as made of N parallel infinite lines of electric charge of the same type, positive or negative, constrained to lie in a plane, with the outermost lines fixed in place but the inner ones free to move in-plane to find their equilibrium positions. Each line has the same charge density per unit length.

Referring back to Figure 24, let N be even and number the line charges from 0 to $N-1$ with 0 at $a_0 = 0$ and $a_{N-1} = 1$. The equilibrium distribution will be symmetric about $x = 1/2$ so impose the condition that $a_{N-1-j} = a_j$. The central two charges are at a_m and a_{m+1} where $m = (N-1)$ DIV 2. The net force on charge j is

$$F_j \;=\; \sum_{k=0,k\neq j}^{N-1} \frac{1}{a_k - a_j}.$$

If $k < j$, the force is from charges to the left of j repelling it towards the right, and *vice versa*. At equilibrium all F_j are zero. There are therefore m simultaneous equations to be solved for $a_1, a_2, ..., a_m$.

We can regard the positions a_j and the forces F_j to be respectively components of a position vector $\mathbf{a}$ and a force vector $\mathbf{F}$. I determined the solution using Newton's method, generalising the familiar $x_1 = x_0 - f(x_0)/f'(x_0)$ formula for obtaining an improved estimate x_1 of the root from a previous estimate x_0. One needs the Jacobian matrix of partial derivatives $\partial F_j/\partial a_k$. The formula is

$$\mathbf{J\Delta} = \mathbf{F}$$

where $\Delta_j = a_{j,new} - a_{j,old}$ and

$$\mathbf{J} \;=\; \begin{pmatrix} \dfrac{\partial F_1}{\partial a_1} & \dfrac{\partial F_1}{\partial a_2} & \cdots & \dfrac{\partial F_1}{\partial a_m} \\ \dfrac{\partial F_2}{\partial a_1} & \dfrac{\partial F_2}{\partial a_2} & \cdots & \dfrac{\partial F_2}{\partial a_m} \\ \cdots & \cdots & \cdots & \cdots \\ \dfrac{\partial F_m}{\partial a_1} & \dfrac{\partial F_m}{\partial a_2} & \cdots & \dfrac{\partial F_m}{\partial a_m} \end{pmatrix}$$

The partial derivatives are given by

$$\frac{1}{(1-a_j-a_k)^2} \;-\; \frac{1}{(a_j-a_k)^2}, \qquad j \neq k,$$

$$\frac{2}{(1-2a_j)^2} \;+\; \sum_{k=0,k\neq j}^{m} \frac{1}{(a_k-a_j)^2} + \frac{1}{(1-a_k-a_j)^2}, \qquad j = k.$$

By using these analytic expressions for the Jacobian approximation errors are kept to a minimum. I found that the solution vector was obtained within a small number of iterations to the

specified accuracy. The tolerance on every δ_j was $0\cdot00002$, and in addition a sum-of-squares tolerance of $0\cdot00002/N$ was imposed. Results were checked against calculations for N up to 20 using Mathematica, then calculations up to 500 were made with a bespoke program. This program was primed with the true positions of the mid-charges for $N = 4$, and increased N in steps of 2, obtaining good starting estimates of the a_j at the new N by scaling all the exact positions found so far by $(N-3)/(N-1)$, and adding a new charge at position a_m. In this way the program incremented N in steps of 2 from 6 to 500, achieving the required accuracy at each step so that errors had little opportunity to accumulate.

Having found the equilibrium positions a_j, the spacings were calculated for $j > 0$ as $(a_{j+1} - a_{j-1})/2$. For the first and last charges fixed at 0 and 1, I took each to occupy a length $\pm a_0/2$; that is, to have their domain extend by $a_0/2$ outside the strip. This treats these end charges in a similar way to the others, which each occupy half of the spaces either side of them.

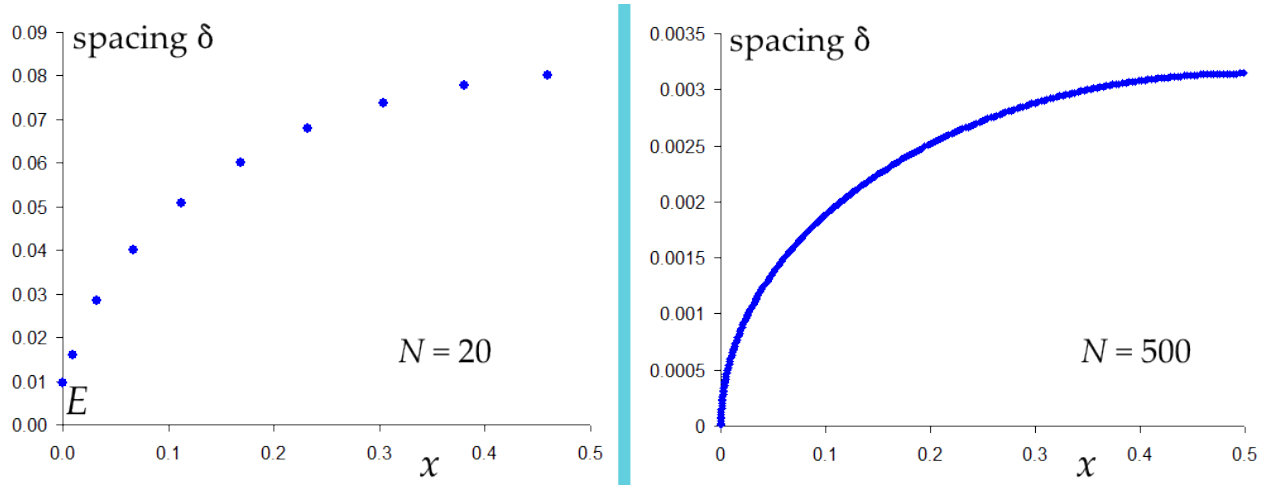

Figure 36: Spacing of 20 and 500 adjacent line charges across strip width 1, showing how their values fit around a quadrant of an ellipse. Strip edge E is at $x = 0$.

I find the result surprising and elegant, that the spacing varies in an ellipsoidal fashion across the strip, with the major axis being the width, 1, of the strip, and also that the minimum spacing is or is close to $\pi/(2N)$. We expect the spacing to fall as $1/N$ as more charges are added, and expect the maximum spacing to exceed $1/N$ since at the edge it is less than this. However, the coefficient $\pi/2 \approx 1\cdot5708$ is probably not to be guessed, and poses a challenge to find a reason in theory. An approach might be to take the limit of $N \to \infty$ and so replace the sum of $1/(a_k - a_j)$ in F_j by an integral. I have not pursued this beyond seeing whether Mathematica can perform

$$\int_0^{a-\epsilon} \frac{1}{(a-x_0)\sqrt{x_0(1-x_0)}}\,dx_0, \qquad \int_{a+\epsilon}^{1} \frac{1}{(x_0-a)\sqrt{x_0(1-x_0)}}\,dx_0$$

to show that these are equal and so cancel to 0 as $\epsilon \to 0$. However, Mathematica fails to return an answer. Perhaps the integral can be done in the complex plane around a contour. I am content that the spacing varies as Eq 22a, b.

Appendix 3: Conducting annulus: equilibrium of rings of charge

This rather long Appendix gives details of the model in §5.3 which extends the method used to find the charge density over a strip to that over an annulus.

A3.1 The model

The annulus is to be made of concentric rings of charge with fixed inner radius R and fixed outer radius $R+1$. We are concerned only with the field in the plane of the rings. Using the formula for the field at radius a_j due to a ring with radius a_k, the total field at radius a_j is found. This is done for every j other than the two fixed rings. The inner rings are allowed to adjust their radii and Newton's method is iterated to find their stable values subject to a small tolerance on convergence. Starting values for Newton's method for N rings are derived from the values already determined for $N-2$. The program starts with only 4 rings and successively adds 2.

The fact that the rings have different radii means that there are two ways in which the charge on each ring can be specified:

1. Option 1: the change per unit arc length λ is the same on all rings,
2. Option 2: the total charge Q on each ring is the same.

A note is in order about the ways of defining charge density. σ is the charge per unit area and λ the charge per unit length of arc. Supposing that a length L of arc carries charge q, the linear density $\lambda = q/L$. If we assign an infinitesimal width $\delta\rho$ to the arc, the area it occupies is $L\,\delta\rho$ and $\sigma = q/(L\,\delta\rho)$. Hence $\lambda = \sigma\,\delta\rho$. In both options σ varies across the conductor on account of the ring spacing varying. In Option 2 the outer rings are weaker than the corresponding ones in Option 1, so in Option 2 the ring spacing at the outer rim will be smaller than in Option 1, but the density of charge per unit area of the annulus, $\sigma(x)$, will be the same. The formulae for potential and field strength plus their partial derivatives (as required by Newton's method) for both options are given below.

The single ring in question has radius ρ and its field is observed at distance x from the central axis which passes through the origin. In the plane of the ring $z = 0$ and $u = 4\rho x/(x+\rho)^2$. From Eq 19c and A1.3 the potential is

$$\text{Option 1}: V = \frac{-4\lambda\rho}{x+\rho} K(u) .$$

$$\text{Option 2}: V = \frac{-2Q}{\pi(x+\rho)} K(u) .$$

Electric field strength in the plane of the ring:

$$\text{Option 1}: |\mathbf{E}| = \frac{2\rho\lambda}{x}\left[\frac{E(u)}{\rho-x} - \frac{K(u)}{\rho+x}\right]$$

$$\text{Option 2}: |\mathbf{E}| = \frac{Q}{\pi x}\left[\frac{E(u)}{\rho-x} - \frac{K(u)}{\rho+x}\right]$$

Partial derivative of field strength with respect to $\rho \equiv a_k$

$$\text{Option 1 : } \frac{\partial \mathbf{E}}{\partial \rho} = \frac{-4\lambda x E(u)}{(\rho - x)^2(\rho + x)},$$

$$\text{Option 2 : } \frac{\partial \mathbf{E}}{\partial \rho} = \frac{-Q}{\pi x \rho(\rho + x))} \left[\frac{(\rho^2 + x^2)}{(\rho^2 - x)^2} E(u) - K(u) \right],$$

Partial derivative of field strength with respect to $x \equiv a_j$

$$\text{Option 1 : } \frac{\partial \mathbf{E}}{\partial x} = \frac{-2\rho\lambda}{x^2(\rho + x)} \left[\frac{(\rho^2 - 3x^2)}{(\rho - x)^2} E(u) - K(u) \right],$$

$$\text{Option 2 : } \frac{\partial \mathbf{E}}{\partial x} = \frac{-Q}{\pi x^2(\rho + x)} \left[\frac{(\rho^2 - 3x^2)}{(\rho - x)^2} E(u) - K(u) \right],$$

I have programmed both options and find that with Option 1 the convergence is generally better. For some radii R the program fails to converge within the required tolerance once N has reached some upper number, which could be over 200 but for other R is as low as 40. The task then is to recognise an analytic function which describes the area charge density over the annulus for all values of R and which therefore takes the correct limiting values at $R \to 0$ and $R \to \infty$.

The first stage in analysis is to demonstrate the equivalence of results under Options 1 and 2. This requires the relation between λ and Q. Under both options the total charge Q_A on the annulus is the same, being $2\pi\lambda \sum a_j$ in Option 1 and NQ in Option 2. To illustrate the matter I selected the annulus with inner radius $0 \cdot 6$ because for this both programs converge for 110 rings, allowing a ring-by-ring comparison. The sum of all ring radii a_j in Option 1 is $131 \cdot 21$ so

$$110\,Q = 2\pi\lambda \sum_{j}^{110} a_j \quad \text{giving} \quad \frac{Q}{2\pi} = 1 \cdot 193\,\lambda. \tag{A3.1}$$

The area density σ for ring j in Option 1 is $\lambda/\delta_{1,j}$ where $\delta_{1,j}$ is the spacing, and in Option 2 is $Q/(2\pi a_{2,j}\delta_{2,j})$. When the densities are scaled by $1 \cdot 193$, the graphs of σ and $1/\sigma$ for the two options are almost coincident, as Figure 37 illustrates. Note how the increased density is concentrated mainly at the outer rim. Eq A3.1 further implies the ring-by-ring correspondence

$$\delta_{1,j} \sum^{N} a_{1,j} = a_{2,j}\,\delta_{2,j}\,. \tag{A3.2}$$

A few numerical checks bear this out.

The next step is to see whether this charge density gives constant potential across the annulus. I used the facility of Mathematica to interpolate between the combined data points in Figure 37 and so by numerical integration to determine the in-plane potential. The result is plotted in Figure 38. The annulus lies between the radii indicated by the red line, and is clearly essentially constant. The slight rounding at the inner and outer rims will be due to an under-estimate of the charge density there, which in theory will tend to being infinite.

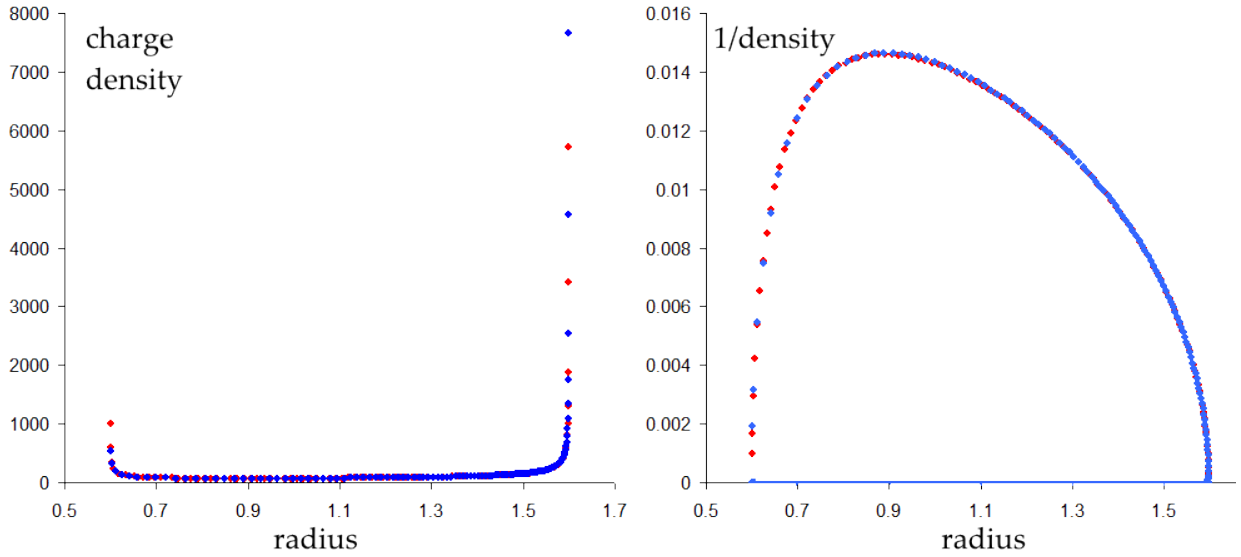

Figure 37: Left: Area charge density σ and, right, reciprocal density for annulus with radii $0 \cdot 6$, $1 \cdot 6$. Red points: Option 1, blue: Option 2.

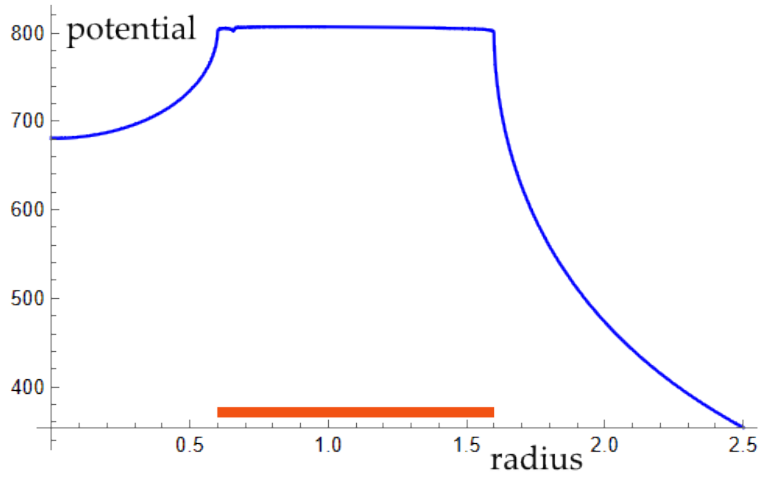

Figure 38: Potential versus radial position through charged annulus, inner radius $0 \cdot 6$.

A3.2 Curve fitting and analytic functions

The result shows that the model does work, but leaves us with the challenge of finding an analytic function which describes the charge density. Most of the rest of this appendix is concerned with curve fitting in the hope that a plausible analytic function for σ will emerge. The graph in the right panel of Figure 37 is not an obvious shape, unlike the ellipse for the strip in Figure 36. Moreover, its shape changes with R. To chart the trend I have calculated the spacing of N rings for a wide range of inner radii R, keeping the outer radii at $R+1$ since this encompasses all shapes of annulus. Calculations were made of the area charge densities $\sigma(x)$ under both Options 1 and 2. A sample for Option 1 is shown in Figure 39, normalised to equal area under each curve. The vertical axis is the width δ_j 'occupied' by ring j at position a_j divided by $\sum \delta_j^2$. The horizontal axis is the distance h across the ring from the inner rim

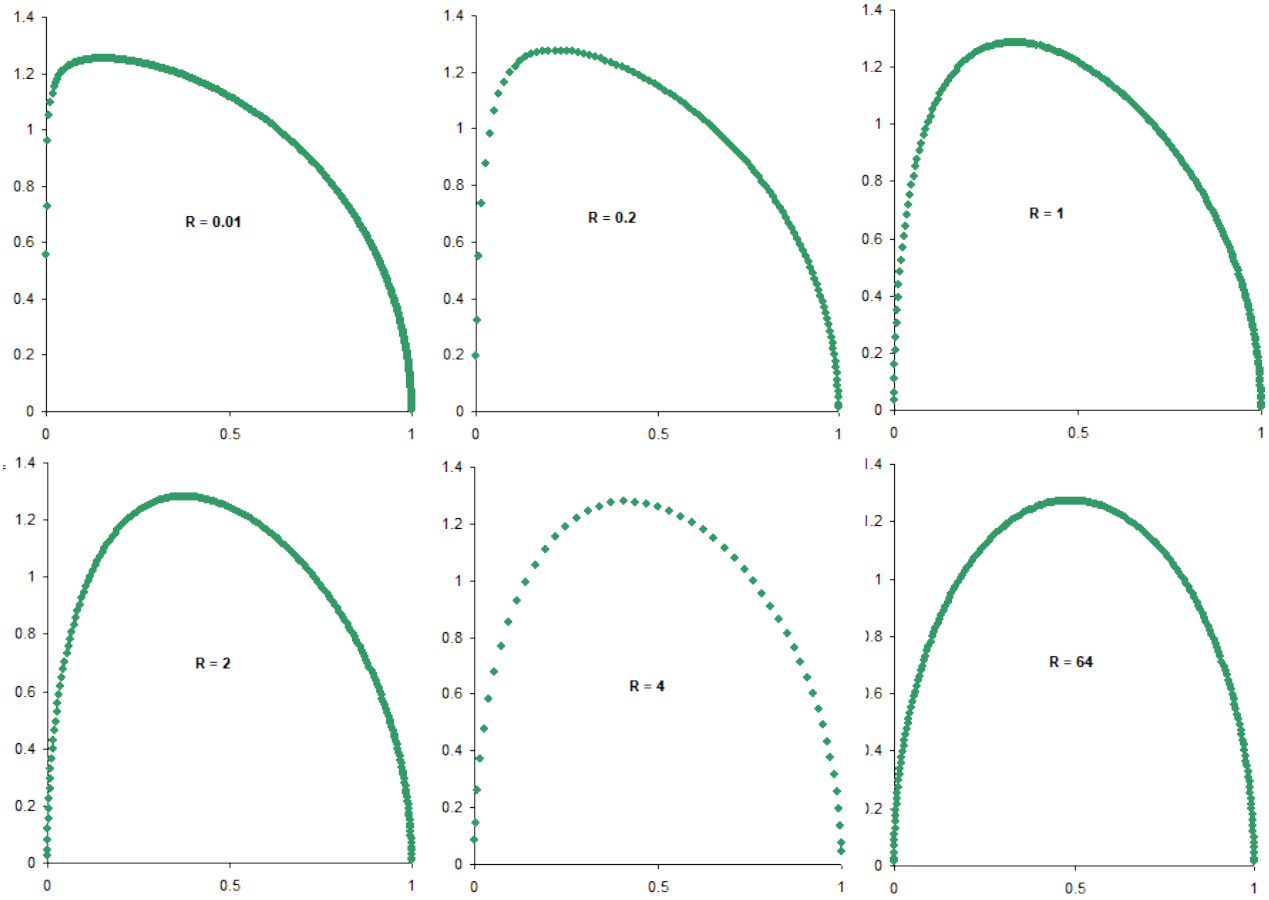

Figure 39: Spacing $d(h)$ between adjacent rings under Option 1 as function of distance from inner rim of annulus, for six values of inner radius R.

($h = x - R$ and is equivalent to $a_j - R$). As $R \to \infty$ the annulus looks like a strip so the curve tends to the upper half of an ellipse as in Figure 36, Appendix 2. At the other extreme of $R \to 0$ the annulus has become a disc with a pin-prick central hole so the curve plotting the ring spacing becomes only the upper right quadrant of an ellipse, as at Figure 23, §5.1.

Clearly the analytic curve expressing the ring spacing δ must be of higher degree than a quadratic conic. One question is 'How does the annulus shrink to a disc?' Does the hole remain a hole until it shrinks to a delta function removed from the disc, or does the hole become bridged in a gradual way. Mathematically, this question is whether all curves like those in Figure 39 fall to zero at $h = 0$ as $R \to 0$. I investigated this by plotting for $R = 0 \cdot 01$ the separation δ_0 of the first two rings at the inner rim as N increases up to 324 using Option 1. The spacing decreases almost linearly with N, and perhaps even shrinks slightly faster than linear. I conclude that the ring spacing at the inner rim does not tend to a constant with N, but continues to decrease roughly as $1/N$, showing that the hole endures.

I have considered curves which are a hybrid of the two limiting forms. For example, Figure 40 shows shapes produced by taking a weighed sum of a) a quarter circle centred about the origin with radius 1, and b) a semicircle centred at $x = 0 \cdot 5$ with diameter 1. Let

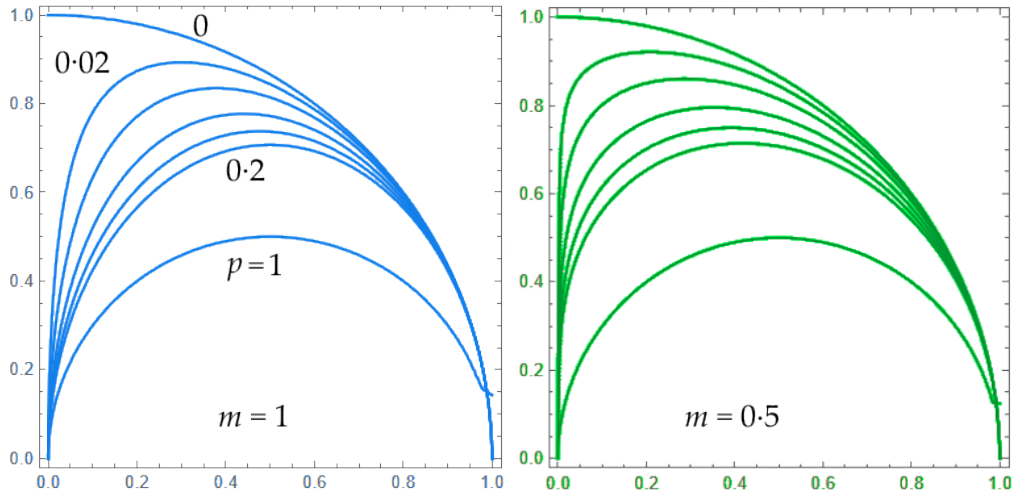

Figure 40: Hybrid curves as candidate models for the ring-spacing graphs of Figure 39.

the distance measured outwards from the inner rim of the annulus be h, so $h = x - R$. The recipe is

$$p(1-h)^m F(h) + (1-p)h^m G(h) = 0, \quad F(h) = 4(h-\tfrac{1}{2})^2 + 4y^2 - 1, \quad G(h) = h^2 + y^2 - 1. \quad (A3.3)$$

These are not simple averages, but weighted in h so that each curve is zero at both ends, the strength of the h-weighting being controlled by the exponent m. Subsequent experience with curves of this type, described below, leads me to judge that simply $m = 1$. I also considered curves of the form $pF(h) + (1-p)hG(h) = 0$, but these do not have symmetry between the two limiting forms and, though close, are not quite such good fits to the numerical curves of $\delta(h)$. I shall therefore be using Eq A3.3 with $m = 1$.

To quantify the model, recall from §4.4 that the capacitance of a conducting disc of radius a is $2a/\pi$. (This is proved by Jeans on page 249 of his book, and is reminiscent of the capacitance of an isolated conducting sphere being equal to a.) If we regard a disc of radius $R+1$ as being composed of a central disc of radius R and an annulus of width 1, both raised to unit potential, then the charge on the inner disc is $2R/\pi$ and on the combined disc is $2(R+1)/\pi$, leaving the annulus with charge $Q_A = 2/\pi$ irrespective of its radius. The smaller disc and annulus are effectively connected electrically in parallel to form the larger disc. In Option 2 this means that the charge Q on each ring is $2/(N\pi)$ units. In Option 1 the total charge is $2\pi\lambda\sum^N a_j$ as at Eq A3.1, so the charge density depends on the sum of radii, which is effectively the total arc length of the charged rings which constitute the annulus. I have obtained a fair approximation to the value of $\sum^N a_j$ in the form $\sum^N a_j/N$. If all rings were equally spaced, $\sum^N a_j/N$ would be $R+\frac{1}{2}$. However, the bunching of rings near the outer rim increases this by η, a small quantity which is a function of both R and N. I have determined the value of η for R between $0\cdot01$ and 64 and for N from 10 to 300. For all R, η increases monotonically with N, tending towards a limiting constant value $\eta_0(R)$ for each R. As R increases, the increase in η with N becomes less and the limiting value is reached for lower N – say by $N = 100$. Figure 41 is a plot of my estimate of these limiting values η_0 obtained from

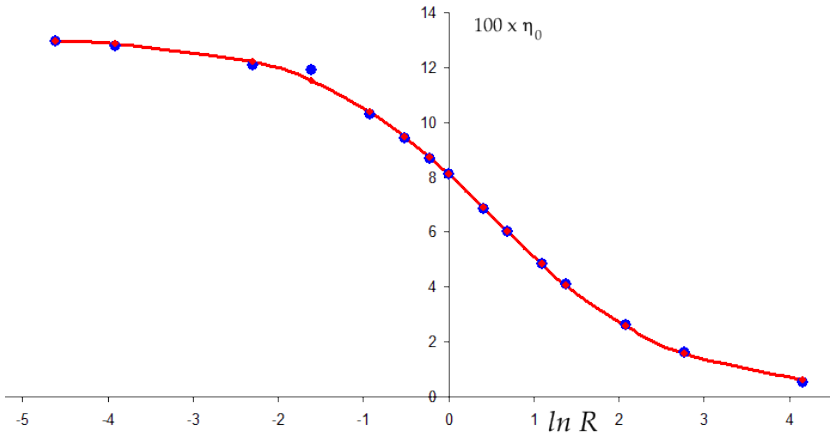

Figure 41: Limiting values of η_0 (×100) versus $\ln R$, allowing calculation of $\sum^N a_j/N = R + \frac{1}{2} + \eta_0$

graphs of η against N. I find that the sigmoidal curve is well approximated by

$$\eta_0 \approx 0 \cdot 066525 - 0 \cdot 06422 \tanh[0 \cdot 47365(\ln R - 0 \cdot 4850)]. \qquad (A3.4)$$

As an example, this means that for $R = 0 \cdot 8, \ln R = -0 \cdot 22314$, the limiting value of $\sum \delta_{1,j} = 0 \cdot 8 + 0 \cdot 5 + 0 \cdot 0873 = 1 \cdot 3875$. For $N = 150$ the actual sum is $1 \cdot 386$ which will be close to but less than the limiting value, η_0.

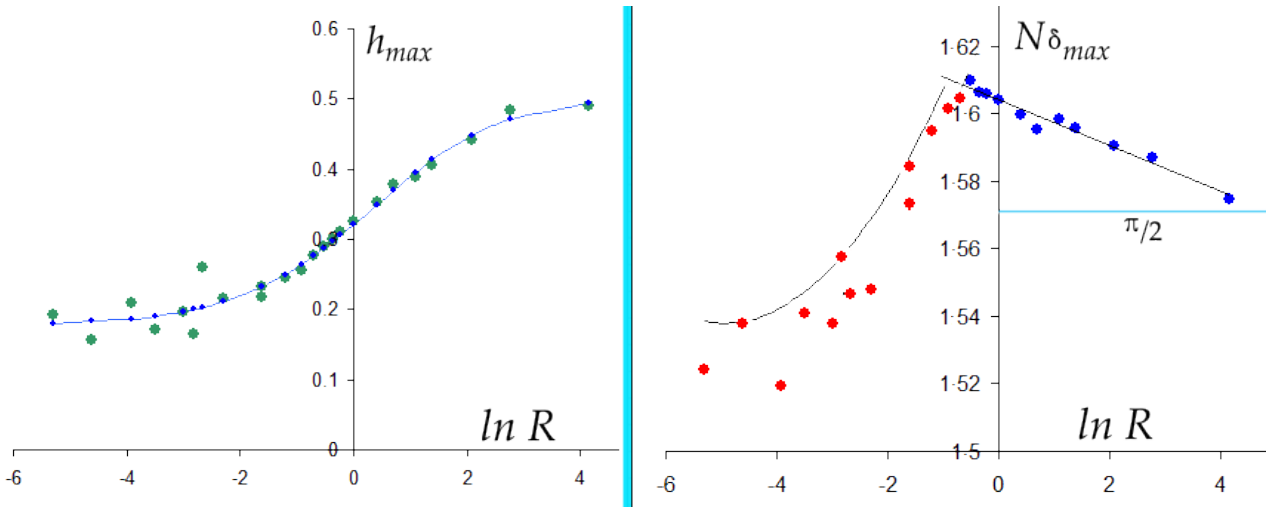

Figure 42: Position and value of largest ring spacing. Left: position h_{max} relative to inner rim. Right: $N\,\delta_{max}$.

It remains to fit analytic functions to the curves such as those in Figure 39 which describe $1/\sigma(R,h)$. The position of the maximum spacing in this curve will be denoted as h_{max} and the peak value as δ_{max}. In Option 1, for which $\sigma = \lambda/\delta$ I have examined the graphs of ring spacing, $\delta(R,h)$, to determine the position of the peak which corresponds to the largest ring spacing. Figure 42 plots numerically determined values for the largest ring spacing δ under Option 1. The left panel shows the peak's position across the annulus from the inner rim. Note how for large R the maximum is half way across at $x = R + 0 \cdot 5$, whereas for very

small R it is around $R + 0\cdot 2$. (Compare with the $R = 0\cdot 01$ curve in Figure 39.) The fitted curve is another arctanh curve:

$$h_{max} \;\approx\; 0\cdot 3424 \,+\, 0\cdot 1648 \tanh(0\cdot 42307 \ln R \,-\, 0\cdot 1288) \qquad (A3.5)$$

The right hand panel in Figure 42 plots the value of the largest spacing, δ_{max}. Since if the rings were equally spaced this spacing would be $1/N$ for large N, the values of δ_j (strictly $\delta_{1,j}$) have been multiplied by N. These normalised values are close to $\pi/2$, but vary as shown in seemingly two different ways. For R less than about $0\cdot 7$ the maximum spacing falls gradually to about $1\cdot 54/N$ (taking the envelope of the points), while for $R > 0\cdot 7$ it falls exponentially to $\pi/2N$.

A3.3 Building analytic expressions

Limit $R = 0$

Collecting what we know, the potential for $R = 0$, when the annulus has contracted to a disc, is obtained as follows. Working in Option 1;

$$i)\ \sigma = \frac{\lambda}{\delta}, \quad ii)\ Q_A = 2\pi\lambda \sum^{N} a_{1,j}\,, \quad iii)\ N\delta_{max} \approx 1\cdot 54 = G.$$

$$iv)\ \sum^{N} a_{1,j} = N\big(R + \tfrac{1}{2} + \eta_0\big) \approx 0\cdot 64N \;=\; gN \text{ for } R = 0,$$

$$v)\ \rho^2 + \frac{\delta^2}{\delta_{max}^2} = 1 \text{ (ellipse) so } \delta = \delta_{max}\sqrt{1-\rho^2}.$$

For shorthand I have introduced the constants g and G and it is tempting to suspect that $gG = 1$ with 'true' values $G = \pi/2 = 1\cdot 571$, $g = 2/\pi = 0\cdot 637$. From this

$$\sigma = \frac{Q_a}{2\pi gN}\frac{N}{G\sqrt{1-\rho^2}} \;=\; \frac{Q_A}{2\pi\sqrt{1-\rho^2}}, \quad R \to 0 \qquad (A3.6)$$

assuming $gG = 1$. This can be checked by integrating the charge density σ over the disc; the value should be Q_A:

$$\int_0^1 2\pi\sigma\rho \; d\rho = 2\pi\frac{Q_A}{2\pi} \;=\; Q_A.$$

This is consistent with the value of σ at Eq 24 of §4.4 and confirms that the graph of ring spacings in Figure 39, in the limit $R \to 0$, is $\delta = \frac{\pi}{2N}\sqrt{1-\rho^2} \;\equiv\; \frac{\pi}{2N}\sqrt{1-h^2}$.

Limit $R \to \infty$

Now for the other limit of $R \to \infty$. Again working in Option 1;

$$i)\ \sigma = \frac{\lambda}{\delta}, \quad ii)\ Q_A = 2\pi\lambda \sum^{N} a_{1,j}\,, \quad iii)\ \delta_{max} = \frac{\pi}{2N},$$

$$iv)\ \sum^{N} a_{1,j} = N\big(R + \tfrac{1}{2} + \eta_0\big) \to N\big(R + \tfrac{1}{2}\big) \text{ for } R \to \infty,$$

$$v)\ 4\big(h - \tfrac{1}{2}\big)^2 + \frac{\delta^2}{\delta_{max}^2} = 1 \text{ (ellipse) so } \delta = \frac{\pi}{N}\sqrt{h(1-h)}.$$

Combining these,

$$\sigma \;=\; \frac{Q_a}{\pi^2(2R+1)}\sqrt{h(1-h}\quad R\to\infty \qquad (A3.7)$$

To check this, integrate over the annulus:

$$\int_0^1 2\pi(R+h)\sigma\; dh \;=\; Q_A\,.$$

A general annulus

The ellipses for δ in the two limits above take the roles of $G(h)$, $F(h)$ in Eq A3.3, so now we look for combinations weighted by the parameter p which fit the observed curves such as those in Figure 39. Try with the exponent m set to 1 for simplicity:

$$p(1-h)\left(4\left(h-\tfrac{1}{2}\right)^2+\frac{4d^2N^2}{\pi^2}-1\right)+(1-p)h\left(h^2+\frac{4d^2N^2}{\pi^2}-1\right) \;=\; 0 \qquad (A3.8a)$$

from which we obtain the ugly expression

$$\delta(h) \;=\; \frac{\pi}{2N}\sqrt{\frac{h^3(1-5p)+8h^2p-h(1+3p)}{2hp-h-p}}\,. \qquad (A3.8b)$$

I will use the position of the peak in this curve to build an estimate of the value of the parameter p corresponding to a given value of annulus inner radius R. The above curve takes the value $\pi/(2N) = 1\cdot5708/N$ for $p = 1$, $h = 0\cdot5$ as required, and also for $p = 0$ as $h \to 0$. However, it is mere conjecture that this formula is a true representation of the spacing of the rings and hence of the charge density. The critical test is whether the value of p deduced for a chosen R leads to the same potential at every position $h = R - x$ across the annulus. An estimate of $p(R)$ can be obtained using the fitted curves in Figure 41, 42. Differentiating Eq A3.8 gives the position h_{max} of the peak in the graph of δ versus h. Even though the expression is extremely complicated, I will state it:

$$h_{max} \;=\; \frac{1}{A}\left(B+\frac{C}{\sqrt[3]{D}}+\sqrt[3]{D}\right), \qquad D = 6p\sqrt{E}+F,$$

$$A \;=\; 6(1-7p+10p^2], \quad B \;=\; p(31p-11), \quad C \;=\; p^2(25-10p+p^2),$$

$$E \;=\; 3(1-8p+17p^2-10p^3)^2\,(27-162p-260p^2+98p^3+196p^4),$$

$$F \;=\; p(54-594p+1711p^2-681p^3-190p^4+1351p^5).$$

The cubic has three roots and all three are required to obtain the required value of h_{max}; there are branch points at $h = 0\cdot2$ and $0\cdot5$. h_{max} is entirely a function of p and is more helpfully shown in a graph of numerical values, left panel of Figure 43. The right panel of the figure shows the values of $\ln p$ which correspond with $\ln R$. This has been derived by using the fitted curve for h_{max} at Eq A3.5. A tanh-type of curve can be fitted to the graph of $\ln p$ against $\ln R$:

$$\ln p \;\approx\; 2\cdot071\tanh(0\cdot4944\ln R\,+0\cdot1341)-2\cdot028. \qquad (A3.9)$$

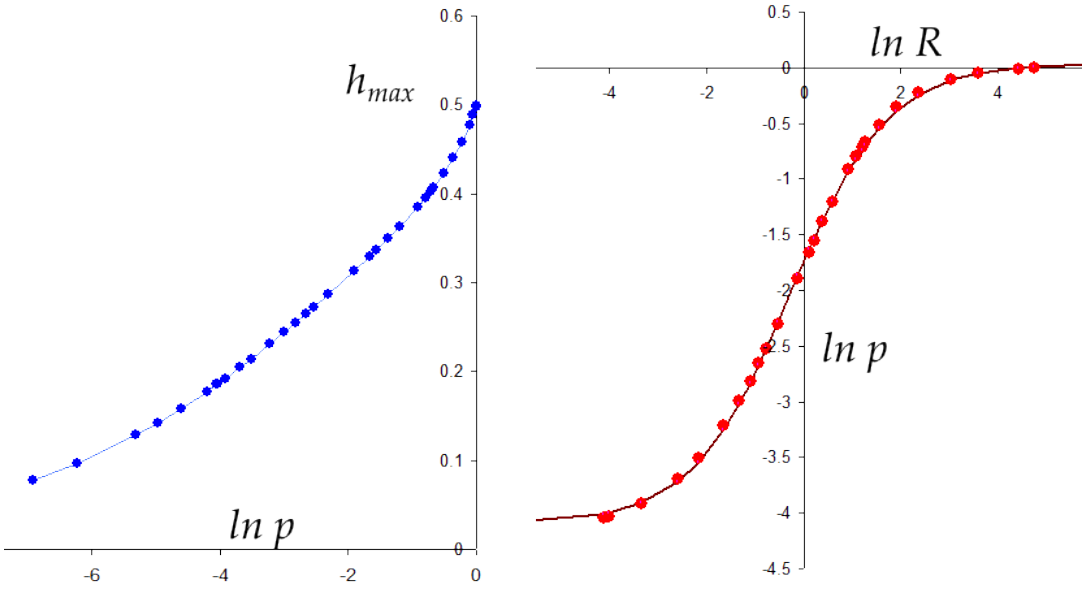

Figure 43: Relations between parameter p and h_{max} (left) and R (right).

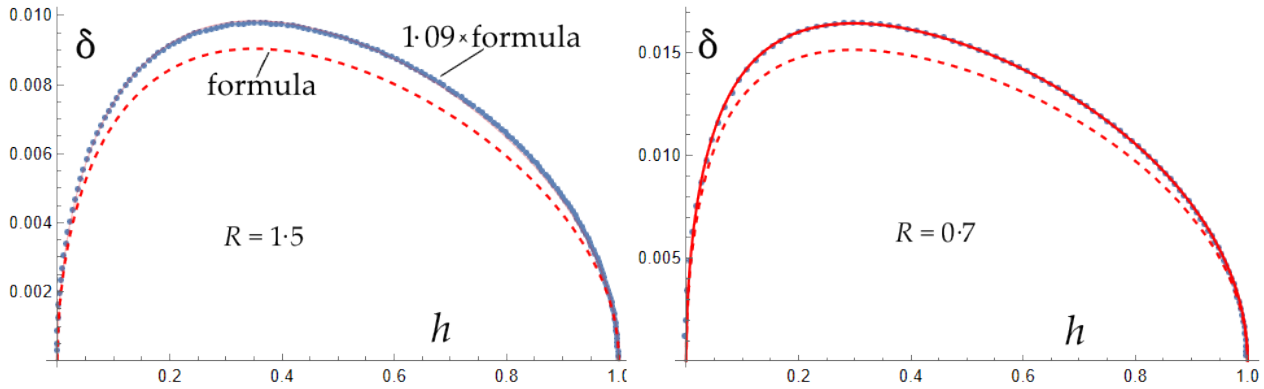

Figure 44: Fitting the model curve (dashed) to the numerical data points.

As an example of using this graph, the approximate value of p from Eq A3.9 when $R = 1 \cdot 5$ is $0 \cdot 257$. Similarly for $R = 0 \cdot 7$ the value is $0 \cdot 119$. To confirm that we are on the right lines, the two panels in Figure 44 plot as dashed red lines the spacings of charged rings within the model for these two values of R. $R = 1 \cdot 5$ has 168 rings and $0 \cdot 7$ has 98, and these values have been input to Eq A3.8b. It is clear that though the curves have the same shape as the numerically calculated spacings (blue dots), the heights are not the same. However by scaling the left panel by $1 \cdot 090$ and the right by $1 \cdot 085$, good agreement is achieved (solid red lines).

Using these two R values as examples, calculation of $\sigma(h)$ for a general annulus is as follows. Working in Option 1;

$$i)\ \sigma = \frac{\lambda}{\delta}, \quad ii)\ Q_A = 2\pi\lambda \sum^{N} a_{1,j},$$

$$iii)\ \sum^{N} a_{1,j} = N(R+\tfrac{1}{2}+\eta_0)\ =\ gN: \quad g \approx 2\cdot 07N \text{ for } R = 1\cdot 5,\ 1\cdot 29 \text{ for } R = 0\cdot 7,$$

$$iv)\ \delta = \frac{B\pi}{2N}\sqrt{\frac{h^3(1-5p)+8h^2p-3hp-h}{2hp-h-p}} \quad \text{with } p \approx 0\cdot 257 \text{ for } R = 1\cdot 5,\ 0\cdot 119 \text{ for } R = 0\cdot 7.$$

$$v)\ \sigma\ =\ \frac{Q_A J}{\pi^2 H(R+\frac{1}{2})}, \quad H(R+\tfrac{1}{2}) = gB, \quad J\ =\ \sqrt{\frac{2hp-h-p}{h^3(1-5p)+8h^2p-3hp-h}}.$$

Note that

$$\lim_{R\to 0} J = \frac{1}{\sqrt{1-h^2}}, \qquad \lim_{R\to\infty} J = \frac{1}{2}\frac{1}{\sqrt{h(1-h)}}$$

since $p \to 0$ as $R \to 0$ and $p \to 1$ as $R \to \infty$. I have introduced the scale factor B which is $1\cdot 09$ for $R = 1\cdot 5$ to bring the formula for $\delta(h)$ into agreement with the numerical values for 168 rings. It is reasonable to combine B with factor g to produce a single scale factor H which fits the constraints. However, since $g \approx R + 0\cdot 5$, I have set $H = gB/(R+0\cdot 5)$ to obtain a number which is not far from being constant.

An important constraint is that the total charge on the annulus be Q_A:

$$Q_A \int_0^1 2\pi(R+h)\sigma(h)\ dh.$$

The values of g and B for $R = 1\cdot 5$ would give $H = 2\cdot 07 \times 1\cdot 09/(1\cdot 5 + 0\cdot 5) = 1\cdot 128$, whilst the integration would requite $H = 1\cdot 139$. This and similar discrepancies are relatively small. I will work on the principle that the total charge must be correct and so have calculated the corresponding value for $H(R)$ for several R. These are plotted in the left panel of Figure 45. The wobbles in this curve probably reflect deviations of the model from the true reciprocal charge density. I split the curve into two sections:

$$\text{For } R < 0\cdot 6,\ \ln R < -0\cdot 5, \quad H \approx 1\cdot 196 - 0\cdot 0763\tanh(0\cdot 5607\ln R + 0\cdot 7724),$$

$$\text{For } R > 0\cdot 6,\ \ln R > -0\cdot 5, \quad H \approx 1\cdot 151 - 0\cdot 0312\ln R. \qquad (A3.11)$$

Regarding the parameter p, which sets the shape of the charge density distribution as a function of the inner radius R, a first estimate was made in the right panel in Figure 43. This gives the values of p which place the peak of the curve $\delta(h)$ in the same position as does the ring model. I have since recalculated p to that which gives the best least-squares fit to the whole $\delta(h)$ curve, and this is plotted in the right panel of Figure 45. The confused bunch of points around $\ln R = -5$ arise because the model curve J cannot fit exactly to the ring spacings from the computer model. However, p must tend to 0 with R so I have introduced the one isolated point at the bottom left. Regarding numerical values, it is appropriate to split the wide range of R into three overlapping sub-ranges with these approximations for p:

$$\text{For } R < 0\cdot 35,\ \ln R < -1\cdot 0, \quad \ln p \approx 0\cdot 69\ln R - 1\cdot 95, \qquad (A3.10)$$

$$\text{For } 0\cdot 2 < R < 4,\ -1\cdot 6 < \ln R < 1\cdot 4, \quad \ln p \approx 0\cdot 916\ln R - 1\cdot 694,$$

$$\text{For } R > 1\cdot 5,\ \ln R > 0\cdot 5, \quad \ln p \approx 0\cdot 987\tanh(0\cdot 916\ln R - 0\cdot 687) - 0\cdot 987.$$

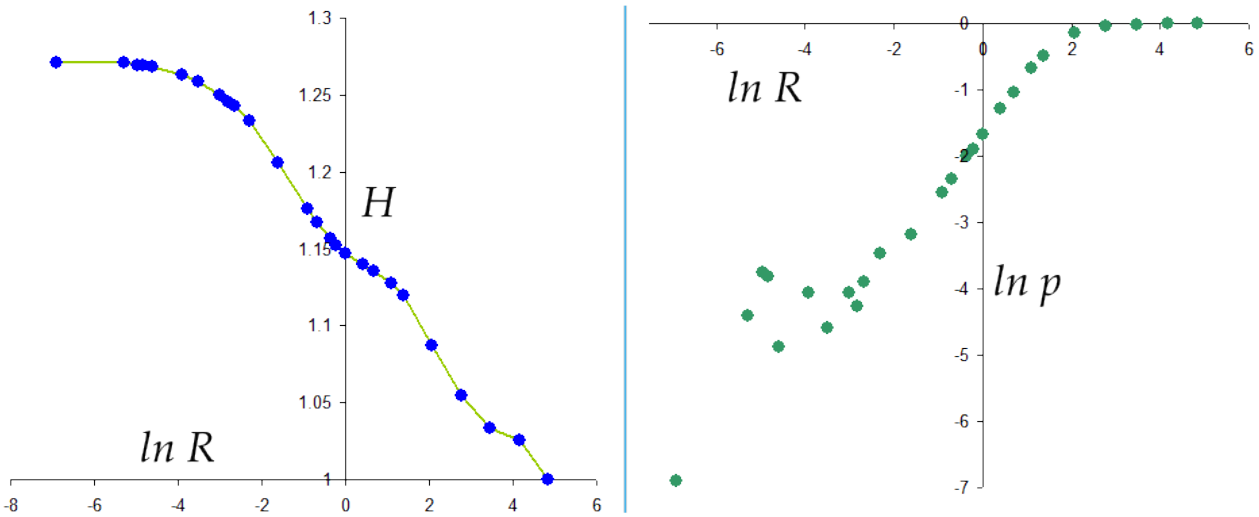

Figure 45: Dependence of the parameters p and H on inner radius R. Left: log-log plot of p versus R. Right: H versus $\ln R$.

This essentially completes the model and my proposal for an approximation to the charge density across an annulus and hence the potential on its surface. In summary, the charge density $\sigma(h)$ varies with position h from the inner rim, radius R, according to

$$\sigma = \frac{Q_A J}{\pi^2 H(R+\frac{1}{2})}, \qquad J = \sqrt{\frac{2hp-h-p}{h^3(1-5p)+8h^2p-3hp-h}}. \tag{A3.12}$$

Numerical values for parameter p and the scale factor H can be read from Figure 45 or evaluated from the fitted curves at Eqs A3.10 and A3.11 respectively. The potential in the plane of the annulus is

$$V(x,0) = \int_0^1 \frac{4\sigma(R+h)}{x+R+h} K\left(\frac{4x(R+h)}{(R+h+x)^2}\right) dh\,. \tag{A3.13}$$

The test of the whole model is to calculate the potential across annuli of different shapes to see whether each has constant potential. As three examples, take $R = 0\cdot09$, 1 and 3.

Case 1: $R = 0{\cdot}09$ **:** $\ln R = -2{\cdot}408$. From Eq A3.11 $H = 1{\cdot}236$ and from Eq A3.12 $\ln p = -3{\cdot}611$, $p = 0{\cdot}0270$. The left panel of Figure 46 shows the potential across the annulus for this value of p. It is not quite constant and has a noticeable peak at the inner rim. By reducing p, and so adding charge near the inner rim, the graph can be flattened as the right panel for $p = 0\cdot016$ shows. One could make a third revision of p as a function of R by experimenting with such plots, but I have resisted the temptation to do so. The theoretical value of potential on a disc with radius $1\cdot09$ is $\pi/2\cdot18 = 1\cdot441$, and the values at $x = 0\cdot5$, at the centre of the annulus, are $1\cdot446$ for $p = 0\cdot027$ and $1\cdot443$ for $p = 0\cdot016$.

Case 2: $R = 1$ **:** $\ln R = 0$. $H = 1\cdot147$ and $p = 0\cdot186$. The left panel of Figure 47 shows the potential. It is convincingly flat a=over the annulus.

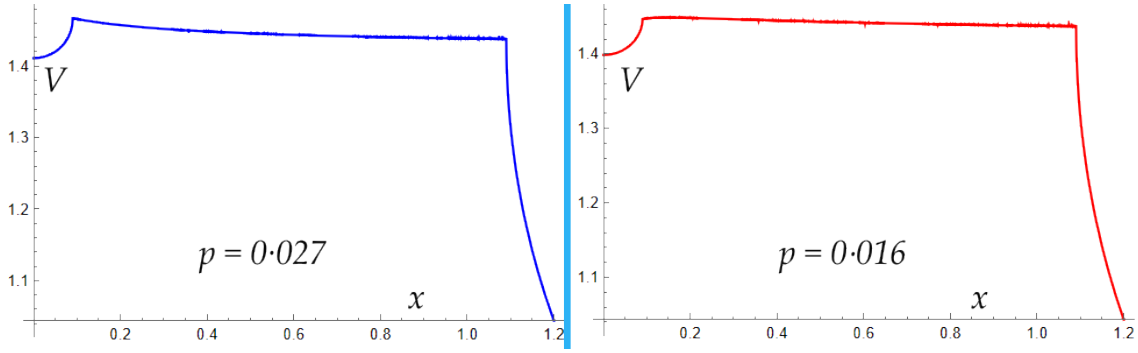

Figure 46: Potential in plane of annulus $R = 0 \cdot 09$ with two values of shape parameter p.

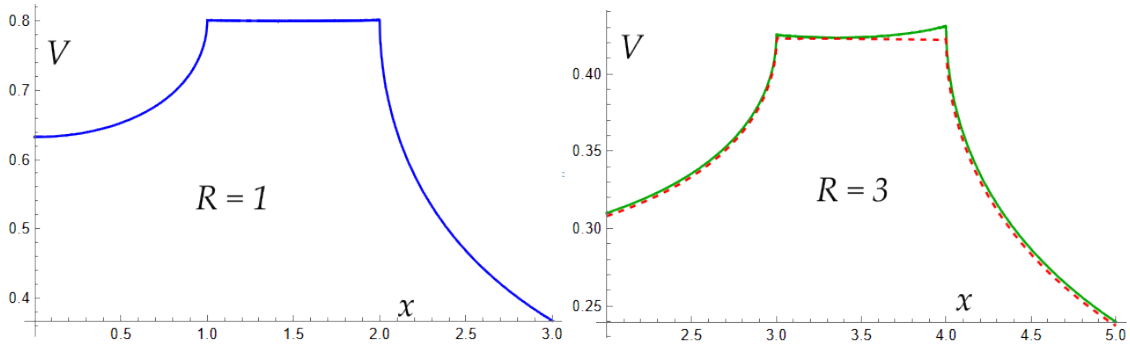

Figure 47: Potential for annuli of inner radii $R = 1$ and $R = 3$. Red dashed curve: using ring model data. Solid green curve: using fitted analytic curves.

Case 3: $R = 3$ **:** $\ln R = 1 \cdot 099$. $H = 1 \cdot 128$ and $p = 0 \cdot 508$. The solid green curve in the right panel of Figure 47 shows the potential using the fitted curves. It clearly sags in the middle and rises to the outer rim, meaning that the charge density here is too low in the middle, too high at the outer rim. However, this is a consequence of imprecise approximation in the fitted curve $J(h)$, as the red dashed curve shows. This was calculated from table of ring densities from the computer model, interpolated to give σh. With is, the potential across the annulus is almost constant.

In conclusion, the charge density and hence potential across an annulus can be modelled quite well by an arrangement of many concentric charged rings whose equilibrium spacing has been calculated. An attempt to summarise the modelled charge distribution by fitted curves has moderate success, though the proposed shape function $J(h, R)$ is an inelegant expression, a hybrid between the two limiting forms of the curve at $R = 0$ and $R \to \infty$. The potential at a general external point is.

$$V(x,z) \;=\; \int_0^1 \frac{4\sigma(R+h)}{\sqrt{(x+R+h)^2+z^2}} K\left(\frac{4x(R+h)}{(R+h+x)^2+z^2}\right) dh\,. \qquad (A3.14)$$